SYNTHESIS AND CHARACTERIZATION OF ZINC OXIDE NANOWIRE

BY

IGORI WALLACE
(PG/M.SC/09/50717)

DEPARTMENT OF PURE AND INDUSTRIAL CHEMISTRY
FACULTY OF PHYSICAL SCIENCES
UNIVERSITY OF NIGERIA, NSUKKA

JANUARY, 2013

SYNTHESIS AND CHARACTERIZATION OF ZINC OXIDE NANOWIRE

BY

IGORI, WALLACE
(PG/M.SC/ 09/ 50717)

A RESEARCH PROJECT SUBMITTED IN PARTIAL FULFILMENT OF THE REQUIREMENT FOR THE AWARD OF THE DEGREE OF MASTER OF SCIENCE IN INDUSTRIAL CHEMISTRY IN THE DEPARTMENT OF PURE AND INDUSTRIAL CHEMISTRY, FACULTY OF PHYSICAL SCIENCES, UNIVERSITY OF NIGERIA, NSUKKA.

JANUARY, 2013

APPROVAL PAGE

This research project has been approved by the Department of Pure and Industrial Chemistry, Faculty of Physical Sciences, University of Nigeria, Nsukka.

---	---
PROF. P.O. UKOHA	PROF. U.C. OKORO

HEAD OF DEPARTMENT

DATE é é é é é é é é .

PROJECT SUPERVISOR

DATE é é é é é é é é .

CERTIFICATION

I certify that this project work titled ñ Synthesis and Characterization of Zinc Oxide Nanowireò was carried out by Igori Wallace, Registration Number; PG/M.Sc/09/50717 under my supervision and is hereby approved as an original work for the Department of Pure and Industrial Chemistry, University of Nigeria, Nsukka.

é é é é é é é é é é é .
IGORI WALLACE

PROF. U.C. OKORO
PROJECT SUPERVISOR

DATE é é é é é é é é .

PROF. P.O. UKOHA
HEAD OF DEPARTMENT

DATE é é é é é é é é .

EXTERNAL EXAMINER

DATE é é é é é é é é .

DEDICATION

This work is dedicated to Almighty God, my father Chief (Hon) Godwin Owulo and my mother Owulo Abigail (Mrs).

ACKNOWLEDGEMENT

I express my sincere thanks to my supervisor, Prof. U.C. Okoro of the Department of Pure and Industrial Chemistry, University of Nigeria, Nsukka for his esteemed supervision, incessant support, inspiration and constructive criticism throughout my project work.

I extend my sincere gratitude and appreciation to my friends; Hilary Abuh, Dr. Oluwa, Mr. George Agocha, Master James Obahi, Mr. Omenka Ajom, Mr. Jude Onyomo, Mr. Ogujor Lagidoese, Mr. Jacob Omenka, Master Victor Okpashi, Obinna Oje, Dr. Parker, Sunday Agbo e.t.c. for their support and encouragement toward my academic success.

I am highly indebted to all the lecturers in Department of Pure and Industrial Chemistry, University of Nigeria, Nsukka for their fatherly advice, knowledge inculcation and encouragement towards the success of this programme.

Special thanks are due to my course mates; Emma, Evans, Gloria, Austin, Peace, etc for their help in one form or the other to ensure the success and realization of this programme.

I must appreciate my beloved wife, Charity Ugboji for being there for me all the time.

Finally, I would also express my deep sense of gratitude to my parents and family members for their encouragement and support throughout, which always inspired me.

ABSTRACT

Zinc Oxide (ZnO) nanowires with hexagonal structure were successfully synthesized by chemical bath deposition technique. The obtained nanowires were characterized by scanning electron microscope (SEM), X-ray diffraction (XRD), energy dispersive X-ray analysis (EDX) and spectrophotometer. The SEM micrographs revealed the morphology of ZnO nanowires with diameter between 170.3 and 481nm and showed that the pH of the bath solution, 8.1 is the optimized value to form ZnO nanowires with hexagonal shape. The XRD pattern of the samples revealed that ZnO nanowire has a hexagonal crystallite structure and further showed that the crystallite size supported by Scherrer's equation increase with increasing annealing temperature (0.536 nm, 0.541nm, 0.557 nm at 100^0C, 150^0C and 200^0C) respectively. The EDX analysis revealed the elemental compositions of samples and confirmed the presence of Zn and O. The results of the optical analysis showed that ZnO nanowire has high absorbance in the ultraviolet and infrared regions with high transmittance in the visible region. The results further revealed that the absorbance of the nanowire increase with increasing annealing temperature. Its high absorbance in the ultraviolet region suggest that it can be use as solar harvester for trapping solar energy for photovoltaic panel which is capable of converting sunlight radiation directly to electricity for commercial or industrial purpose.

LIST OF FIGURES

LIST OF TABLE

TABLE OF CONTENTS

ABBREVIATIONS

AAO	Anodic Aluminum Oxide
APCVD	Atmospheric Pressure Chemical Vapor Deposition
CNFETs	Carbon Nanotube Field-Effect Transistors
CNTs	Carbon Nanotubes
CBD	Chemical Bath Deposition
CBE	Chemical Beam Epitaxy
CVD	Chemical Vapor Deposition
DFT	Density Functional Theory
EL	Electroluminescence
EDX	Energy Dispersive X-Ray
FET	Field-Effect Transistors
HRTEM	High-Resolution Transmission Electron Microscopy
IUPAC	International Union of Pure and Applied Chemistry
LED	Light Emitting Diodes
LPCVD	Low-Pressure Chemical Vapour Deposition

MCM	Mobile Crystalline Material
MOCVD	Metal-Organic Chemical Vapour Deposition
MOS	Metal Oxide Semiconductor
MWNTs	Mult-Walled Nanotubes
pH	Potential of Hydrogen
PL	Photoluminescence
PVD	Physical Vapour Deposition
PLD	Pulsed Laser Deposition
SEM	Scanning Electron Microscope
SWNTs	Single-Walled Nanotubes
TMCH	Transition-Metal/Chalcogen/Halogenides
UV	Ultraviolet Radiation
VPE	Vapour Phase Epitaxy
VSLE	Vapour-Liquid-Solid Epitaxial
XRD	X-Ray Diffraction

CHAPTER ONE
INTRODUCTION

1.1 **Background of the Research**

Nanoscience evolution and the advent of nanowire fabrication marked a new epoch in optoelectronics [1]. Characteristic investigation for achieving efficient light absorption, charge separation transport and collection had culminated in the synthesis of both organic and inorganic semiconductor nanowires [2-3]. The d-block transition elements of the periodic table are all metals of economic importance. Zinc, which is a group II element, finds numerous potential applications, such as smart windows, solar thermal absorber, optical memories and photoelectrocatalysis [4-5].

Nowadays, the products of semiconductor industry are spread all over the world and deeply penetrate into the daily life of humans. The starting point of semiconductor industry was the invention of the first semiconductor transistor in 1947.[3] Since then, the semiconductor industry has kept growing enormously. In the 1949ôs, the information age of humans was started on the basis of the stepwise appearance of quartz optical fiber, group III-V compound semiconductors and gallium arsenide (GaAs) lasers. During the development of the information age, silicon (Si) keeps the dominant place on the commercial market, which is used to fabricate the discrete devices and integrated circuits for computing, data storage and communication. Since Si has an indirect band-gap which is not suitable for optoelectronic devices such as light emitting diodes (LEDs) and laser diodes, GaAs with direct band-gap stands out and fills the blank for this application. As the development of information technologies continued, the requirement of ultraviolet (UV)/blue light emitter applications became stronger and stronger which is beyond the limits of GaAs. Therefore, the wide band-gap semiconductors such as gallium nitride (GaN) and zinc oxide (ZnO), i.e. the third generation semiconductors, come forth and turn into the research focus in the field of semiconductor.

ZnO is a typical II-VI semiconductor material with a wide band-gap of 3.37 eV at room temperature. Although its band-gap value is closer to GaN (3.44eV), its exciton binding energy is as high as 39eV, which is much higher than that of GaN (25eV). Therefore, theoretically, we can harvest high efficient UV exciton emission and laser at room temperature, which will strongly prompt the applications of UV laser in the fields of benthal

detection, communication and optical memory with magnitude enhancement in the performance. Moreover, the melting point of ZnO is 1954^0C, which determines its high thermal and chemical stability. Again, ZnO owns a huge potentially commercial value due to its cheaper price, abundant resources in nature, environmentally friendly, simple fabrication processes and so on. Therefore, ZnO has turned into a new hot focus in the field of short-wavelength laser and optoelectronic devices in succession to GaN in the past decade.

It is believed by many researchers that ZnO is a more prospective candidate for the next generation of light emitters for solid state lighting applications than GaN, even though the GaN-based LEDs have been commercialised and currently dominated the light emission applications in UV/blue wavelength range. This is because ZnO has several advantages compared to GaN. The two outstanding factors are;

1. The exciton binding energy of ~39eV at room temperature is much higher than that of GaN (~25eV), which can enhance the luminescence efficiency of ZnO based light emission devices at room temperature, and lower the threshold for lasing by optical pumping. [6-7]

2. The growth of high quality single crystal substrates is easier and of lower cost than GaN.[6-7]

Increasingly interesting properties and potential applications of ZnO have been discovered. One of the most attractive aspects is that it is relatively simple for ZnO to form various nanostructures including highly ordered nanowire arrays, tower-like structures, nanorods, nanobelts, nanosprings and nanorings [8]. Due to the special physical and chemical properties derived from the nanostructures, ZnO has been found to be promising in many other applications, such as sensing [9-10], catalysis [11-12], photovoltaics [13] and nano-generators [14-16], just to mention but a few.

In order to utilize the applications of nanostructure materials, it usually requires that the crystalline morphology, orientation and surface architecture of nanostructures can be well controlled during the preparation processes. For ZnO nanostructures, although different fabrication methods such as vapor-phase transport [17], pulsed laser deposition [18], chemical vapor deposition and electrochemical deposition,[19] have been widely used to prepare ZnO nanostructures, the complex processes, sophisticated equipments and high temperature requirement make them very hard for large-scale production for commercial application. On the contrary, aqueous chemical method is of great advantage due to much easier operation and very low growth temperature (95^0C) [20]. ZnO nanostructures grown by this method show poor

orientation and different crystalline structures due to the fact that, the optimum conditions required for the growth of these nanostructures is still grossly understudied. Hence, it is still a significant challenge to obtain controllable growth of ZnO nanostructures. It is therefore imperative to investigate the various conditions necessary for the growth of well align ZnO nanostructures.

1.2. NANOWIRES

A nanowire is a nanostructure, with the diameter of the order of a nanometer (10^{-9} meters). Alternatively, nanowires can be defined as structures that have a thickness or diameter constrained to tens of nanometers or less and an unconstrained length [21]. At these scales, quantum mechanical effects are important ð which coined the term "quantum wires". Many different types of nanowires exist, including metallic (e.g., Ni, Pt, Au), semiconducting (e.g., Si, InP, GaN, ZnO, etc.), and insulating (e.g., SiO_2, TiO_2).

Typical nanowires exhibit ratios (length-to-width ratio) of 1000 or more. As such they are often referred to as one-dimensional (1-D) materials. Nanowires have many interesting properties that are not seen in bulk or 3-D materials. This is because electrons in nanowires are quantum confined laterally and thus occupy energy levels that are different from the traditional continuum of energy levels or bands found in bulk materials. Peculiar features of this quantum confinement exhibited by certain nanowires manifest themselves in discrete values of the electrical conductance. Such discrete values arise from a quantum mechanical restraint on the number of electrons that can travel through the wire at the nanometer scale [21].

Nanowires also show other peculiar electrical properties due to their size. Unlike carbon nanotubes, whose motion of electrons can fall under the regime of ballistic transport (meaning the electrons can travel freely from one electrode to the other), nanowire conductivity is strongly influenced by edge effects. The edge effects come from atoms that lay at the nanowire surface and are not fully bonded to neighboring atoms like the atoms within the bulk of the nanowire. The unbonded atoms are often a source of defects within the nanowire, and may cause the nanowire to conduct electricity more poorly than the bulk material. As a nanowire shrinks in size, the surface atoms become more numerous compared to the atoms within the nanowire, and edge effects become more important.

Furthermore, the conductivity can undergo a quantization in energy: i.e. the energy of the electrons going through a nanowire can assume only discrete values, multiple of the Von

Klitzing constant (G) = $2e^2/h$ (where e is the charge of the electron and h is the Planckôs constant). The conductivity is hence described as the sum of the transport by separate channels of different quantized energy levels. The thinner the wire is, the smaller the number of channels available to the transport of electrons.

The quantized conductivity is more pronounced in semiconductors like Si or GaAs than in metals, due to lower electron density and lower effective mass. Quantized conductance can be observed in 25 nm wide silicon fins, resulting in increased threshold voltage. [21]

1.2.1. Applications of Nanowire

In addition to variations in size and material, nanowire research also spans a wide range of applications.

1.2.1.2. Gas Sensor

Nanowire sensors have been demonstrated to detect the presence of many gases, including oxygen [22], hydrogen, NO_2, and ammonia [23], at very low concentrations. Nanowires also have been used to detect ultraviolet light [24], changes in pH [25], and the presence of low-density lipoprotein cholesterol [26]. These sensors generally function by measuring changes in the electrical or physical properties of the nanowire in the presence of the target analyte. The sensing capabilities of nanowires may be enabled by selective doping or by surface modifications that enhance their affinities for certain substances.

1.2.1.3. Medical Applications

Nanowires have been used to coat titanium implants. [27] Doctors have discovered that muscle tissues sometimes do not adhere well to titanium, but when coated with the nanowires, the tissue can anchor itself to the implant, reducing the risk of implant failure. Nanowires are used for the production of nanoscale sensors for various purposes, one of which is in the detection of potential biomarkers of cancer. For example, nano-sized sensing wires that are laid across a microfluid channel can pick up molecular signatures of the particles and can relay the information instantaneously and these sensors can detect altered genes that are associated with cancer and ultimately have the potential to provide information on the location of the malignant genes [28]. Nanowires also play important roles in nano-size devices like nanorobots. Doctors could use the nanorobots to treat diseases like cancer [29].

1.2.1.4. Magnetic Storage Medium

The most attractive potential applications of nanowires lie in the magnetic information storage medium. Studies have shown that periodic arrays of magnetic nanowire arrays possess the capability of storing forty gigabytes of information per square centimeter of area ($40G/cm^2$) [30]. The small diameter, single domain nanowires of Ni, Co fabricated into the pores of porous anodic alumina has been found to be most suitable for the above purpose. The high aspect ratio of the nanowires results in enhanced coercivity and suppresses the onset of the ósuperparamagnetic limitô, which is considered to be very important for preventing the loss of magnetically recorded information between the nanowires. Suitable separation between the nanowires is maintained to avoid the inter-wire interaction and magnetic dipolar coupling. It has been found that nanowires can be used to fabricate stable magnetic medium with packing density > 1011 wires/cm^2 [31].

1.2.1.5. Electronic Applications

Some nanowires are very good conductors or semiconductors, and their miniscule size means that manufacturers could fit millions more transistors on a single microprocessor. As a result, computer speed would increase dramatically. Nanowires possess the potential for use in numerous electronic applications. Junctions of semiconductor nanowires such as GaAs and GaP have shown good rectifying characteristics [32]. Several semiconductor devices such as junction diodes , memory cells and switches [33], transistors, field-effect transistors (FETs), light emitting diodes (LEDs) and inverter [34] etc have already been fabricated using nanowire junctions. The field effect transistors made of nanowires exhibit remarkably modified conductance behaviour [35] and they are very attractive because of their morphological advantages. The operational speed of FETs made of nanowires is much faster compared to that of bulk FETs.

1.2.1.6. Optical Applications

Uniform morphology and interesting optical properties of nanowires have raised their potential for various optical applications. The nï p junction of nanowires has been found to be capable of light emission, by virtue of their photoluminescence (PL) or electroluminescence (EL) properties. The use of pï n junction nanowires has been contemplated for laser applications. It

has been established that ZnO nanowires of wire diameter smaller than the wavelength of emitted light exhibits lasing actions at lower threshold energy compared to their bulk counterpart. [36] This has been attributed to the exciton confinement effect in the laser action, which decreases the threshold lasing energy in nanowires. This effect has been observed in small diameter ZnO (385 nm diameter) and GaN nanowires. The huge surface area and the high conductivity along the length of nanowires are suitable for inorganicï organic solar cell [37].

It is to be noted that when the intensity of the incident photons are increased the electron density of the sub-band edges also increases, due to the above fact, these quantum wires develop strong nonlinearity. Therefore, nanowires may be used to develop optical switches. These optical switches will be able to operate at lower energy and with enhanced switching speed compared to the known switches.

Nanowire can be used in field emission devices such as flat panel displays because of the significant drop in the work function of the surface electrons in those small diameter and high curvature tips of the nanowires [37].

1.3. STATEMENT OF PROBLEM

Literature have shown that, man depend majorly on non-renewable energy source (coal, fossil fuel and natural gas) as the primary energy source. However, the energy generated from these sources is limited and their waste products non-environmentally friendly, costly, and limited in quantity. Because nature does not produce them at the same rate that they are being consumed they are bound to expire one day. Based on this, it is imperative to search for a more abundant, environmentally friendly, clean, cheap and sustainable energy source as an alternative source.

In view of these, the optical property of ZnO nanowire is investigated to find its potency as solar harvester as renewable energy for industrial and commercial purpose.

1.4. AIM AND OBJECTIVES OF THE STUDY

This research work is aimed at synthesizing and characterizing ZnO nanowire and the specific objectives of the study were as follows:

(a) Fabrication of ZnO nanowires using chemical bath deposition method.

(b) Microstructure characterization of deposited ZnO nanowires using SEM, XRD, UV, EDX.

(c) Investigation of the effect of post annealing temperature on the optical property of the grown ZnO nanowires.

(d) Investigation of the effect of pH on the structure and morphology of the synthesized ZnO nanowires.

(e) Determination of the crystallite size of the synthesized ZnO nanowires.

1.5. JUSTIFICATION OF THE STUDY

The growth of ZnO nanowire with hexagonal structure was successfully achieved. These nanowires are useful in varied areas of life to man. Due to its high absorbance in the ultraviolet region of light spectrum, it can be used as solar harvester, smart windows, solar thermal absorber and optical memories. In electronics, nanowires can be use as devices such as junction diodes, memory cells and switches, transistors, FETs, LEDs and inverter. Nanowire can also be used as sensors that can detect the presence of many gases, including oxygen, hydrogen, NO_2, and ammonia, at very low concentrations. They can also be used to detect ultraviolet light, changes in pH, and the presence of low-density lipoprotein cholesterol.

CHAPTER TWO

LITERATURE REVIEW

2.0 NANOMATERIALS

A nanomaterial is a material made up of nanostructures between 1 and 100 nanometres (or billionths of a metre) in size. These nanostructures can be nanoparticles , nanotubes (such as carbon nanotubes), nanowires, nanoporous, nanocomposite or nanocrystals. Because of the small size of the structures that make them up, the properties of nanomaterials are different from those of ordinary materials [38].

2.1. NANOTUBES

A nanotube is a nanometer-scale tube-like structure. Nanotube may be classified as carbon nanotube, inorganic, DNA and membrane nanotubes.

2.1.1. Inorganic Nanotube

An inorganic nanotube is a cylindrical molecule often composed of metal oxides, and morphologically similar to a carbon nanotube. Inorganic nanotubes have been observed to occur naturally in some mineral deposits.[39]

Although Linus Pauling mentioned the possibility of curved layers in minerals as early as 1930, [40] synthetic inorganic nanotubes did not appear until Reshef & his coworkers reported the synthesis of nanotubes composed of tungsten disulfide (WS_2) in 1992.[41]

In the intervening years, nanotubes have been synthesised from many other inorganic materials, such as vanadium oxide and manganese oxide, and are being researched for such applications as redox catalysts and cathode materials for batteries.

SnS_2/SnS nanotubes have been synthesized in macroscopic amounts.[42] However, traditional ceramics like titanium dioxide (TiO_2) and zinc oxide (ZnO) also form inorganic nanotubes.[43] More recent nanotube and nanowire materials are transition_metal/chalcogen/halogenides (TMCH), described by the formula $TM_6C_yH_z$, where TM is transition metal (molybdenum, tungsten, tantalum, niobium), C is chalcogen (sulfur, selenium, tellurium), H is halogen (iodine), and the composition is given by $8.2<(y+z)<10$. TMCH tubes can have a subnanometer-diameter, lengths tunable from hundreds of nanometers to tens of microns and show excellent dispersiveness owing to extremely weak mechanical coupling between the tubes.[44]

In 2007, Chinese scientists announced the fabrication of copper and bismuth nanotubes.[45]

2.1.1.1. Properties and Applications of Inorganic Nanotube

Inorganic nanotubes are an alternative material to better-explored carbon nanotubes, showing advantages such as easy synthetic access and high crystallinity,[46] good uniformity and dispersion, predefined electrical conductivity depending on the composition of the starting material and needle-like morphology, good adhesion to a number of polymers and high impact-resistance.[47] They are therefore promising candidates as fillers for polymer composites with enhanced thermal, mechanical, and electrical properties. Target applications for this kind of

composites are materials for heat management, electrostatic dissipaters, wear protection materials, photovoltaic elements, etc. Inorganic nanotubes are heavier than carbon nanotubes and not as strong under tensile stress, but they are particularly strong under compression, leading to potential applications in impact-resistant applications such as bulletproof vests.[47]

2.1.2. Carbon Nanotube

Carbon nanotubes (CNTs) are allotropes of carbon with a cylindrical nanostructure. Nanotubes have been constructed with length-to-diameter ratio of up to 132,000,000:1,[48] significantly larger than any other material. These cylindrical carbon molecules have unusual properties, which are valuable for nanotechnology, electronics, optics and other fields of materials science and technology. In particular, owing to their extraordinary thermal conductivity and mechanical and electrical properties, carbon nanotubes find applications as additives to various structural materials. For instance, in (primarily carbon_fiber) "baseball bats, car parts" and even "golf clubs" [48], where nanotubes form only a tiny portion of the material(s).

Nanotubes are members of the fullerene structural family, which also includes the spherical buckyballs, and the ends of a nanotube may be capped with a hemisphere of the buckyball structure. Their name is derived from their long, hollow structure with the walls formed by one-atom-thick sheets of carbon, called graphene. These sheets are rolled at specific and discrete ("chiral") angles, and the combination of the rolling angle and radius decides the nanotube properties; for example, whether the individual nanotube shell is a metal or semiconductor. Nanotubes are categorized as single-walled nanotubes (SWNTs) and mult-walled nanotubes (MWNTs). Individual nanotubes naturally align themselves into "ropes" held together by van der Waals forces, more specifically, pi-stacking.

Applied quantum chemistry, specifically, orbital hybridization best describes chemical bonding in nanotubes. The chemical bonding of nanotubes is composed entirely of sp^2 bonds, similar to those of graphite. These bonds, which are stronger than the sp^3 bonds found in alkanes, provide nanotubules with their unique strength.

Most single-walled nanotubes (SWNT) have a diameter of close to 1 nanometer, with a tube length that can be many millions of times longer. The structure of a SWNT can be conceptualized by wrapping a one-atom-thick layer of graphite called graphene into a seamless

cylinder. The way the graphene sheet is wrapped is represented by a pair of indices (*n*,*m*) . The integers *n* and *m* denote the number of unit vectors along two directions in the honeycomb crystal lattice of graphene. If *m* = 0, the nanotubes are called zigzag nanotubes, and if *n* = *m*, the nanotubes are called armchair nanotubes. Otherwise, they are called chiral. The diameter of an ideal nanotube can be calculated from its (n,m) indices as follows

$$d = \frac{a}{\pi}\sqrt{(n^2 + nm + m^2)}$$

where a = 0.246 nm.

One useful application of SWNTs is in the development of the first intramolecular field-effect transistors (FET). Production of the first intramolecular logic gate using SWNT FETs has recently become possible as well. [49]

Single-walled nanotubes are dropping precipitously in price, from around $1500 per gram as of 2000 to retail prices of around $50 per gram of as-produced 40ï 60% by weight SWNTs as of March 2010. [50]

Shown below are structures of single-walled carbon nanotube.

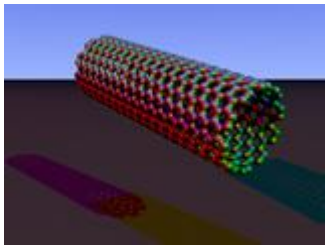

(a) Armchair (*n*,*n*)

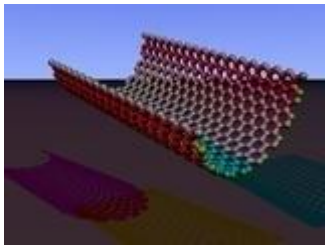

(b) The translation vector is bent, while the chiral Vector stays straight.

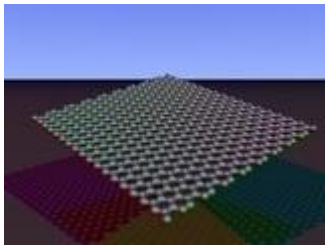

(c)Graphene nanoribbon

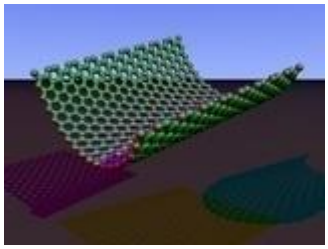

(d) The chiral vector is bent, while the translation

vector stays straight.

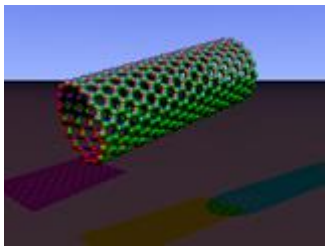

(e)Zigzag (*n*,0)

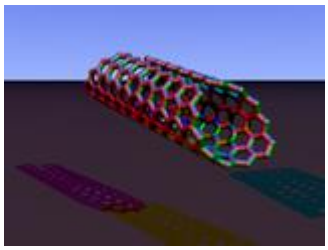

(f) Chiral (*n*,*m*)

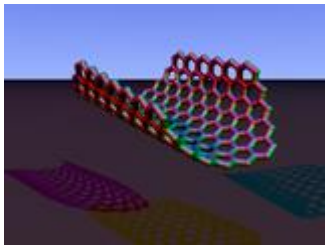

(g)n and *m* can be counted at the end of the tube

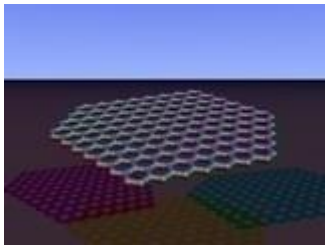

(h) Graphene nanoribbon

Fig.1. Types of single-walled carbon nanotube

Multi-walled nanotubes (MWNT) consist of multiple rolled layers (concentric tubes) of graphite. Its individual shells can be described as SWNTs, which can be metallic or semiconducting. Because of statistical probability and restrictions on the relative diameters of the individual tubes, one of the shells, and thus the whole MWNT, is usually a zero-gap metal.

Double-walled carbon nanotubes (DWNTs) form a special class of nanotubes because their morphology and properties are similar to those of SWNT but their resistance to chemicals is significantly improved. This is especially important when functionalization is required (this means grafting of chemical functions at the surface of the nanotubes) to add new properties to the CNT. In the case of SWNT, covalent functionalization will break some C=C double bonds, leaving "holes" in the structure on the nanotube and, thus, modifying both its mechanical and electrical properties. In the case of DWNT, only the outer wall is modified. DWNT synthesis on the gram-scale was first proposed in 2003 by the CVD technique, from the selective reduction of oxide solutions in methane and hydrogen. [51]

The observation of the longest carbon nanotubes (18.5 cm long) was reported in 2009. These nanotubes were grown on Si substrates using an improved chemical vapor deposition (CVD) method and represent electrically uniform arrays of single-walled carbon nanotubes.[48]

The shortest carbon nanotube is the organic compound cycloparaphenylene, which was synthesized in early 2009.[52]

The thinnest freestanding single-walled carbon nanotube is about 4.3 Å in diameter. Researchers suggested that it can be either (5,1) or (4,2) SWCNT, but exact type of carbon nanotube remains questionable. (3,3), (4,3) and (5,1) carbon nanotubes (all about 4 Å in diameter) were unambiguously identified using more precise aberration-corrected high-resolution transmission electron microscopy. However, they were found inside double-walled carbon nanotubes.[53]

2.1.2.1. Properties of Carbon Nabnotube

2.1.2.1.1. Strength

Carbon nanotubes are the strongest and stiffest materials yet discovered in terms of tensile strength and elastic modulus respectively. This strength results from the covalent sp^2 bonds formed between the individual carbon atoms. In 2000, a multi-walled carbon nanotube was tested to have a tensile strength of 63 gigapascals (GPa).[54] Further studies, conducted in 2008, revealed that individual CNT shells have strengths of up to ~100 GPa, which is in good agreement with quantum/atomistic models.[55] Since carbon nanotubes have a low density for a solid of 1.3 to 1.4 g/cm^3, its specific strength of up to 48,000 $kN \cdot m \cdot kg^{-1}$ is the best of known materials, compared to high-carbon steel's 154 $kN \cdot m \cdot kg^{-1}$.[55]

Under excessive tensile strain, the tubes will undergo plastic deformation, which means the deformation is permanent. This deformation begins at strains of approximately 5% and can increase the maximum strain the tubes undergo before fracture by releasing strain energy.

Although the strength of individual CNT shells is extremely high, weak shear interactions between adjacent shells and tubes leads to significant reductions in the effective strength of multi-walled carbon nanotubes and carbon nanotube bundles down to only a few GPaôs.[55] This limitation has been recently addressed by applying high-energy electron irradiation, which crosslinks inner shells and tubes, and effectively increases the strength of these materials to ~60 GPa for multi-walled carbon nanotubes and ~17 GPa for double-walled carbon nanotube bundles.[55]

CNTs are not nearly as strong under compression. Because of their hollow structure and high aspect ratio, they tend to undergo buckling when placed under compressive, torsional, or bending stress.[56]

2.1.2.1.2. Hardness

Standard single-walled carbon nanotubes can withstand a pressure up to 24GPa without deformation. They then undergo a transformation to superhard phase nanotubes. Maximum pressures measured using current experimental techniques are around 55GPa. However, these new superhard phase nanotubes collapse at an even higher, *albeit* unknown, pressure. The bulk modulus of superhard phase nanotubes is 462 to 546 GPa, even higher than that of diamond (420 GPa for single diamond crystal). [57]

2.1.2.1.3. Kinetic

Multi-walled nanotubes are multiple concentric nanotubes nested within one another. These exhibit a striking telescoping property in which an inner nanotube core may slide, almost without friction, within its outer nanotube shell, thus creating an atomically perfect linear or rotational bearing. This is one of the first true examples of molecular nanotechnology, with the precise positioning of atoms to create useful machines. Already, this property has been utilized to create

the world's smallest rotational motor.[58] Future applications such as a gigahertz mechanical oscillator are also envisaged.

2.1.2.1.4. Thermal

All nanotubes are expected to be very good thermal conductors along the tube, exhibiting a property known as "ballistic conduction", but good insulators laterally to the tube axis. Measurements show that a SWNT has a room-temperature thermal conductivity along its axis of about 3500 $W \cdot m^{-1} \cdot K^{-1}$,[59] when compared to copper, a metal well known for its good thermal conductivity, which transmits 385 $W \cdot m^{-1} \cdot K^{-1}$. A SWNT has a room-temperature thermal conductivity across its axis (in the radial direction) of about 1.52 $W \cdot m^{-1} \cdot K^{-1}$,[60] which is about as thermally conductive as soil.

2.1.2.1.5. Optical

The optical properties of carbon nanotubes refer specifically to the absorption, photoluminescence, and Raman spectroscopy of carbon nanotubes. Spectroscopic methods offer the possibility of quick and non-destructive characterization of relatively large amounts of carbon nanotubes. There is a strong demand for such characterization from the industrial point of view: numerous parameters of the nanotube synthesis can be changed, intentionally or unintentionally, to alter the nanotube quality. Optical absorption, photoluminescence and Raman spectroscopies allow quick and reliable characterization of this "nanotube quality" in terms of non-tubular carbon content, structure (chirality) of the produced nanotubes, and structural defects. Those features determine nearly any other properties such as optical, mechanical, and electrical properties.

Carbon nanotubes are unique "one dimensional systems" which can be envisioned as rolled single sheets of graphite (or more precisely graphene). This rolling can be done at different angles and curvatures resulting in different nanotube properties. The diameter typically varies in the range 0.4ï 40 nm (i.e. "only" ~100 times), but the length can vary ~10,000 times reaching 18.5 cm. Thus the nanotube aspect ratio, or the length-to-diameter ratio, can be as high as 132,000,000:1,[60] which is unequalled by any other material. Consequently, all the properties of

the carbon nanotubes relative to those of typical semiconductors are extremely anisotropic (directionally dependent) and tunable.

2.1.2.2. Methods of Synthesis

Techniques have been developed to produce nanotubes in sizeable quantities, including arc discharge, laser ablation and chemical vapor deposition (CVD). Most of these processes take place in vacuum or with process gases. CVD growth of CNTs can occur in vacuum or at atmospheric pressure. Large quantities of nanotubes can be synthesized by these methods; advances in catalysis and continuous growth processes are making CNTs more commercially viable.

2.1.2.2.1. Arc Discharge

Nanotubes were observed in 1991 in the carbon soot of graphite electrodes during an arc discharge, by using a current of 100 amps, that was intended to produce fullerenes. However the first macroscopic production of carbon nanotubes was made in 1992 by two researchers at NEC's (national electrical code) Fundamental Research Laboratory.[61] The method used was the same as in 1991. During this process, the carbon contained in the negative electrode sublimates because of the high-discharge temperatures. Because nanotubes were initially discovered using this technique, it has been the most widely-used method of nanotube synthesis. The yield for this method is up to 30% by weight and it produces both single- and multi-walled nanotubes with lengths of up to 50 micrometers with few structural defects.[62]

2.1.2.2.2. Laser Ablation

In the laser ablation process, a pulsed laser vaporizes a graphite target in a high-temperature reactor while an inert gas is bled into the chamber. Nanotubes develop on the cooler surfaces of the reactor as the vaporized carbon condenses. A water-cooled surface may be included in the system to collect the nanotubes.

The laser ablation method yields around 70% and produces primarily single-walled carbon nanotubes with a controllable diameter determined by the reaction temperature. However, it is more expensive than either arc discharge or chemical vapor deposition.[62]

2.1.2.2.3. Chemical Vapor Deposition (CVD)

During CVD, a substrate is prepared with a layer of metal catalyst particles, most commonly nickel, cobalt, iron, or a combination.[63] The metal nanoparticles can also be produced by other ways, including reduction of oxides or oxides solid solutions. The diameters of the nanotubes that are to be grown are related to the size of the metal particles. This can be controlled by patterned (or masked) deposition of the metal, annealing, or by plasma etching of a metal layer. The substrate is heated to approximately 700°C. To initiate the growth of nanotubes, two gases are bled into the reactor: a process gas (such as ammonia, nitrogen or hydrogen) and a carbon-containing gas (such as acetylene, ethylene, ethanol or methane). Nanotubes grow at the sites of the metal catalyst; the carbon-containing gas is broken apart at the surface of the catalyst particle, and the carbon is transported to the edges of the particle, where it forms the nanotubes. This mechanism is still being studied. The catalyst particles can stay at the tips of the growing nanotube during the growth process, or remain at the nanotube base, depending on the adhesion between the catalyst particle and the substrate. Thermal catalytic decomposition of hydrocarbon has become an active area of research and can be a promising route for the bulk production of CNTs. Fluidised bed reactor is the most widely used reactor for CNT preparation. CVD is a common method for the commercial production of carbon nanotubes. For this purpose, the metal nanoparticles are mixed with a catalyst support such as MgO or Al_2O_3 to increase the surface area for higher yield of the catalytic reaction of the carbon feedstock with the metal particles. One issue in this synthesis route is the removal of the catalyst support via an acid treatment, which sometimes could destroy the original structure of the carbon nanotubes. However, alternative catalyst supports that are soluble in water have proven effective for nanotube growth.[64]

Of the various means for nanotube synthesis, CVD shows the most promise for industrial-scale deposition, because of its price/unit ratio, and because CVD is capable of growing nanotubes directly on a desired substrate, whereas the nanotubes must be collected in the other growth techniques. The growth sites are controllable by careful deposition of the catalyst. Researchers at Rice University, until recently led by the late Richard Smalley, have concentrated upon finding methods to produce large, pure amounts of particular types of nanotubes. Their approach grows long fibers from many small seeds cut from a single nanotube; all of the resulting fibers were

found to be of the same diameter as the original nanotube and are expected to be of the same type as the original nanotube.[65]

2.1.2.3. Potential Applications

The strength and flexibility of carbon nanotubes makes them of potential use in controlling other nanoscale structures, which suggests they will have an important role in nanotechnology engineering. The highest tensile strength of an individual multi-walled carbon nanotube has been tested to be 63 GPa.[54]

Because of the carbon nanotube's superior mechanical properties, many structures have been proposed ranging from everyday items like clothes and sports gear to combat jackets and space elevators.[66] However, the space elevator will require further efforts in refining carbon nanotube technology, as the practical tensile strength of carbon nanotubes can still be greatly improved.[62]

Carbon nanotubes are also a promising material as building blocks in bio-mimetic hierarchical composite materials given their exceptional mechanical properties (~1TPa in modulus, and ~100 GPa in strength). Initial attempts to incorporate CNTs into hierarchical structures led to mechanical properties that were significantly lower than these achievable limits. Windle et al.[67] have used an *in situ* chemical vapor deposition (CVD) spinning method to produce continuous CNT yarns from CVD grown CNT aerogels. With this technology, they fabricated CNT yarns with strengths as high as ~9 GPa at small gage lengths of ~1 mm, however, defects resulted in a reduction of specific strength to ~1 GPa at 20 mm gage length.

Solar cells developed at the New Jersey Institute of Technology use a carbon nanotube complex, formed by a mixture of carbon nanotubes and carbon buckyballs (known as fullerenes) to form snake-like structures. Buckyballs trap electrons, although they can't make electrons flow. If sunlight is added to excite the polymers, the buckyballs will grab the electrons. Nanotubes, behaving like copper wires, will then be able to make the electrons or current flow.[68]

2.1.3. MEMBRANE NANOTUBES

Membrane nanotubes or cytonemes are long and thin tubes formed from the plasma membrane that connect different animal cells over long distances, and could sometimes extend for over 100

εm between T cells.[69] Two types of nanotubes have been observed. The first type are less than 0.7 micrometres in diameter, contain actin and carry portions of plasma membrane between cells in both directions. The second type are larger (>0.7 εm), contain both actin and microtubules and can carry components of the cytoplasm between cells, such as vesicles and organelles.[70]

These structures may be involved in cell-to-cell communication, transfer of nucleic acids between cells in a tissue,[71] and the spread of pathogens or toxins such as HIV.[69] Membrane nanotubes were first described in a 1999 *Cell* article examining the development of *Drosophila melanogaster* wing imaginal discs.[72] More recently, a *Science* article published in 2004 described structures that connected various types of immune cell together, as well as connections between cells in tissue culture.[73]

2.1.4. DNA NANOTUBE

DNA nanotubes are hollow tubes formed of strands of DNA that are a few nanometers wide. They are somewhat similar in size and shape to carbon nanotubes, but the carbon nanotubes are stronger and better conductors, whereas the DNA nanotubes are more easily modified and connected to other structures.

In the far future these nanotubes might be used as ñmagic bulletsò that deliver drugs locally to specific diseased cells. Genes in the cell then trigger the release of the encapsulated cargo. [74]

2.2. NANOCOMPOSITE

A nanocomposite is as a multiphase solid material where one of the phases has one, two or three dimensions of less than 100 nanometers (nm), or structures having nano-scale repeat distances between the different phases that make up the material.[75] In the broadest sense this definition can include porous media, colloids, gels and copolymers, but is more usually taken to mean the solid combination of a bulk matrix and nano-dimensional phase(s) differing in properties due to dissimilarities in structure and chemistry. The mechanical, electrical, thermal, optical, electrochemical, catalytic properties of the nanocomposite will differ markedly from that of the component materials. Size limits for these effects have been proposed,[76] <5 nm for catalytic activity, <20 nm for making a hard magnetic material soft, <50 nm for refractive index changes,

and <100 nm for achieving superparamagnetism, mechanical strengthening or restricting matrix dislocation movement.

Nanocomposites differ from conventional composite materials due to the exceptionally high surface to volume ratio of the reinforcing phase and/or its exceptionally high aspect_ratio. The reinforcing material can be made up of particles (e.g. minerals), sheets (e.g. exfoliated clay stacks) or fibres (e.g. carbon nanotubes or electrospun fibres). The area of the interface between the matrix and reinforcement phase(s) is typically an order of magnitude greater than for conventional composite materials. The matrix material properties are significantly affected in the vicinity of the reinforcement.[75] Note that with polymer nanocomposites, properties related to local chemistry, degree of thermoset cure, polymer chain mobility, polymer chain conformation, degree of polymer chain ordering or crystallinity can all vary significantly and continuously from the interface with the reinforcement into the bulk of the matrix. This large amount of reinforcement surface area means that a relatively small amount of nanoscale reinforcement can have an observable effect on the macroscale properties of the composite. For example, adding carbon nanotubes improves the electrical and thermal conductivity. Other kinds of nanoparticulates may result in enhanced optical properties, dielectric properties, heat resistance or mechanical properties such as stiffness, strength and resistance to wear and damage. In general, the nano reinforcement is dispersed into the matrix during processing. The percentage by weight (called *mass fraction*) of the nanoparticulates introduced can remain very low (on the order of 0.5% to 5%) due to the low filler percolation threshold, especially for the most commonly used non-spherical, high aspect ratio fillers (e.g. nanometer-thin platelets, such as clays, or nanometer-diameter cylinders, such as carbon nanotubes).

2.2.1. Classification of Nanocomposite

2.2.1.1. Ceramic-Matrix Nanocomposites

In this group of composites the main part of the volume is occupied by a ceramic, i.e. a chemical compound from the group of oxides, nitrides, borides, silicides etc. In most cases, ceramic-matrix nanocomposites encompass a metal as the second component. Ideally both components, the metallic one and the ceramic one, are finely dispersed in each other in order to elicit the

particular nanoscopic properties. Nanocomposites from these combinations were demonstrated in improving their optical, electrical and magnetic properties[77] as well as corrosion-resistance and other protective properties.[78]

The concept of ceramic-matrix nanocomposites was also applied to thin films that are solid layers of a few nm to some tens of µm thickness deposited upon an underlying substrate and that play an important role in the functionalization of technical surfaces. Gas flow sputtering by the hollow cathode technique turned out as a rather effective technique for the preparation of nanocomposite layers. The process operates as a vacuum-based deposition technique and is associated with high deposition rates up to some µm/s and the growth of nanoparticles in the gas phase. Nanocomposite layers in the ceramics range of composition were prepared from TiO_2 and Cu by the hollow cathode technique [79] that showed a high mechanical hardness, small coefficients of friction and a high resistance to corrosion.

2.2.1.2. Metal-Matrix Nanocomposites

Metal matrix nanocomposites can also define as reinforced metal matrix composites.This kind of composites can be classify as continous and non continous reinforced materials. One of the important nanocomposites is Carbon nanotube metal matrix composites which is emerging new materials that are being developed to take advantage of the high tensile strength and electrical conductivity of carbon nanotube materials. Critical to the realization of CNT-MMC (carbon nanotube metal matrix composite) possessing optimal properties in these areas are the development of synthetic techniques that are (a) economically producible, (b) provide for a homogeneous dispersion of nanotubes in the metallic matrix, and (c) lead to strong interfacial adhesion between the metallic matrix and the carbon nanotubes.In addition to carbon nanotube metal matrix composites , boron nitride reinforced metal matrix composites and carbon nitride metal matrix composites are the new research areas on metal matrix nanocomposites.[80]
Another kind of nanocomposite is the energetic nanocomposite, generally as a hybrid solï gel with a silica base, which, when combined with metal oxides and nano-scale aluminium powder, can form superthermite materials.[80]

2.2.1.3. Polymer-Matrix Nanocomposites

In the simplest case, appropriately adding nanoparticulates to a polymer matrix can enhance its performance, often in very dramatic degree, by simply capitalizing on the nature and properties of the nanoscale filler (these materials are better described by the term ***nanofilled polymer composites***). [81] This strategy is particularly effective in yielding high performance composites, when good dispersion of the filler is achieved and the properties of the nanoscale filler are substantially different or better than those of the matrix, for example, reinforcing a polymer matrix by much stiffer nanoparticles [81] of ceramics, clays, or carbon nanotubes. Alternatively, the enhanced properties of high performance nanocomposites may be mainly due to the high aspect ratio and/or the high surface area of the fillers,[82] since nanoparticulates have extremely high surface area to volume ratios when good dispersion is achieved.

Nanoscale dispersion of filler or controlled nanostructures in the composite can introduce new physical properties and novel behaviours that are absent in the unfilled matrices, effectively changing the nature of the original matrix (such composite materials can be better described by the term ***genuine nanocomposites*** or ***hybrids*** [81]). Some examples of such new properties are fire resistance or flame retardancy and accelerated biodegradability.

2.2.2. Areas of Application

Such mechanical property improvements have resulted in major interest in nanocomposite materials in numerous automotive and general/industrial applications. These include potential for utilisation as mirror housings on various vehicle types, door handles, engine covers and intake manifolds and timing belt covers. More general applications currently being considered include usage as impellers and blades for vacuum cleaners, power tool housings, mower hoods and covers for portable electronic equipment such as mobile phones, pagers etc.

2.2.2.1. Oxygen Barriers

Honeywell have also been active in developing a combined active/passive oxygen barrier system for polyamide-6 materials. Passive barrier characteristics are provided by nanoclay particles incorporated via melt processing techniques whilst the active contribution comes from an oxygen scavenging ingredient (undisclosed). Oxygen transmission results reveal substantial benefits provided by nanoclay incorporation in comparison to the base polymer (rates approximately 15-20% of the bulk polymer value, with further benefits provided by the combined active/passive

system). Akkapeddi suggests that the increased tortuosity provided by the nanoclay particles essentially slows transmission of oxygen through the composite and drives molecules to the active scavenging species resulting in near zero oxygen transmission for a considerable period of time.[83]

2.2.2.2. Food Packaging

Triton Systems and the US Army are conducting further work on barrier performance in a joint investigation and tested a non-refrigerated packaging system capable of maintaining food freshness for three years. Nanoclay polymer composites are currently showing considerable promise for this application. It is likely that excellent gaseous barrier properties exhibited by nanocomposite polymer systems will result in their substantial use as packaging materials in future years.

2.2.2.3. Films

The presence of filler incorporation at nano-levels has also been shown to have significant effects on the transparency and haze characteristics of films. In comparison to conventionally filled polymers, nanoclay incorporation has been shown to significantly enhance transparency and reduce haze. With polyamide based composites, this effect has been shown to be due to modifications in the crystallisation behaviour brought about by the nanoclay particles; spherilitic domain dimensions being considerably smaller. Similarly, nano-modified polymers have been shown, when employed to coat polymeric transparency materials, to enhance both toughness and hardness of these materials without interfering with light transmission characteristics. An ability to resist high velocity impact combined with substantially improved abrasion resistance was demonstrated by Haghighat of Triton Systems. [83]

2.2.2.4. Flammability Reduction

The ability of nanoclay incorporation to reduce the flammability of polymeric materials was a major theme of the paper presented by Gilman of the National Institute of Standards and Technology in the US. In his work Gilman demonstrated the extent to which flammability behaviour could be restricted in polymers such as polypropylene with as little as 2% nanoclay

loading. [83] In particular heat release rates, as obtained from cone calorimetry experiments, were found to diminish substantially by nanoclay incorporation. Although conventional microparticle filler incorporation, together with the use of flame retardant and intumescent agents would also minimise flammability behaviour, this is usually accompanied by reductions in various other important properties. With the nanoclay approach, this is usually achieved whilst maintaining or enhancing other properties and characteristics. [83]

2.3. NANOPOROUS MATERIALS

According to the International Union of Pure and Applied Chemistry (IUPAC), [84] porous materials can be classified into three categories: (1) micropores are smaller than 2nm in diameter; (2) mesopores are between 2 to 50 nm;(3) macropores are larger than 50 nm. But this definition is somewhat conflict with the more broadened definition of nanoporous materials. The term ñnanoporousò currently refers to the class of porous materials having pore diameters between 1 and 100 nm. It is noted that nanoporous materials actually encompass some micro and macro porous materials and all mesoporous materials. [85]

Nanoporous materials can bring out many interesting unique properties. The high surface area to volume ratio, large surface area and porosity, versatile surface composition and properties enable the nanoporous materials to be used widely in applications, such as catalysis, chromatography, separation, sensing, biological molecular recognition and purification. [86-87] Furthermore, nanoporous materials, especially inorganic nanoporous materials, which are made of mostly metal oxides, are usually non-toxic, inert, chemically and thermally stable, so they have wide applications where biocompatibility or thermal stability requirements are essential.

2.3.1. Review of nanoparticles

Most syntheses of nanoporous materials reported so far have focused on template-assisted bottom-up processes, including soft templating (chelating agents, surfactants, block copolymers and so on) and hard templating [88-92] (porous alumina, carbon nanotubes and nanoporous materials) methods.

Sol-gel technology has been used extensively in the synthesis of nanoporous materials.The overall sol-gel process, as the name implies, usually involves two stages: precursors initially

form high molecular weight but still soluble oligmeric intermediates, a sol, and the intermediates further link together to form a three-dimensional crosslinked network, a gel. The precursors for a sol-gel reaction could be either inorganic salts or organic compounds, such as metal alkoxides. In a typical sol-gel process, the precursor is subjected to a series of hydrolysis and polymerization reactions to form a colloidal suspension, or a "sol". When the "sol" is cast into a mold, a wet "gel" will form. With further drying and heat-treatment, the "gel" is converted into dense ceramic or glass particles.[93-94]

MCM-41(Mobile Crystalline Material) was the first example of nanoporous sol-gel material synthesized through surfactant templated pathway in the early 1990ôs.[88, 95] Since then, tremendous attention and effort have been made in this research field. This surfactant-templated method proved to be an extremely useful strategy to synthesize nanoporous materials with the following characteristics:

- ✓ High surface areas (> 1000 $m^2 g^{-1}$);
- ✓ Tunable, uniform pore sizes (2-10 nm);
- ✓ Long-range ordered pore structures;
- ✓ Structural stability and so on.

Due to those interesting properties, nanoporous materials synthesized by surfactant templated pathways have been studied for various applications, such as heterogeneous catalysis, separation, optics, electronics and sensing. The synthesis process always involves two conceptually simple steps: first forming the surfactant/inorganic mesophase and second removing the surfactant template molecules from the mesostructure after metal oxide framework formation. But the actual kinetics are much more complicated. A variety of parameters can affect the mesophase formation, such as solvent, temperature, pH value, aging time, initial precursor/water/catalyst ratio, etc.

Even though the surfactant templated pathway has proved to be successful for synthesis of nanoporous materials, some drawbacks have prevented their application in some areas. As an example, some cationic surfactants are toxic and expensive; the synthesis is often achieved under harsh conditions during reactions or the templated removal processes, such as high temperature and pressure, strongly acidic or basic media. For some applications, especially in bioscience and biotechnology, those drawbacks are fatal.

To solve these problems, a novel nonsurfactant templating pathway has been developed.[96-97] Instead of using surfactant molecules as template to direct the nanoporous structure formation, non-surfactant small molecules are applied in this new method to function as template molecules. Those small nonsurfactant molecules include glucose, fructose, maltose, urea, dibenzoyl-L-tartaric acid (DBTA), etc.[96] In general, the nonsurfactant pathway starts with the sol-gel reactions of inorganic precursors, e.g., tetraethyl orthosilicate (TEOS) for silica, in the presence of a non-surfactant compound, e.g. glucose. Upon gelation and drying, nonporous, transparent and monolithic solids can be obtained. The template removal can be easily achieved by simple solvent extraction, which means template molecules can be washed out from silica matrices and leave nanoporous structure.

As described above, the nonsurfactant templating pathway has several important advantages over surfactant-templating pathway. First, the whole process can be done at room temperature. Because the interactions between non-surfactant molecules and inorganic phase are much weaker than surfactant/inorganic phase, the removal of templates can be easily accomplished by solvent extraction at room temperature, avoiding high temperature calcination step in the surfactant-templated pathway. Second, many non-surfactant template molecules, like glucose, fructose and maltose are non-toxic and biofriendly. That makes applications in bioscience and biotechnology feasible. Third, during the whole non-surfactant templated process, no acid, alkaline or even organic solvent is necessary at the point when biological substances are introduced. All these characteristics of non-surfactant templating pathway provide a convenient and effective way to prepare nanoporous materials for various applications, especially in biological applications.

2.3.2. **Applications of Nanoporous Materials**

2.3.2.1. **Environmental Separations**

As the regulatory limits on environmental emissions become more and more stringent, industries have become more active in developing separation technologies that could remove contaminants and pollutants from waste gas and water streams. Adsorbent materials and membranes (typically nanoporous) are increasingly being applied and new adsorbents and membranes are constantly being invented and modified for various environmental applications such as the removal of SO_2, NO and VOCs emissions.[89]

2.3.2.2. Sensors And Actuators

Nanoparticles and nanoporous materials possess large specific surface areas, and high sensitivity to slight changes in environments (temperature, atmosphere, humidity, and light). Therefore such materials are widely used as sensor and actuator materials. Gas sensors reply on the detection of electric resistivity change upon change in gas concentration and their sensitivity is normally dependent on the surface area. Gas sensors based on nanoporous metal oxides such as SnO_2, TiO_2, ZrO_2, and ZnO are being developed and applied in detectors of combustible gases, humidity, ethanol, and hydrocarbons. Zirconia is typically a good sensor material for oxygen.[98]

2.3.2.3. Biological Applications

Nanomaterials that are assembled and structured on the nanometer scale are attractive for biotechnology applications because of the potential to use material topography and the spatial distribution of functional groups to control proteins, cells, and tissue interactions, and also for bioseparations.[99] Nanoporous materials being porous and some often found bio-compatible afford the capability to build enzymatic nanomaterials that mimic natural biological reactions. Immobilizing recombinant enzymes into nanoporous materials can be used for long-lifetime biological reactors for a variety of applications. The possibilities for using enzymes in small-scale reactors for producing drugs, energy, decontaminating wastes, and creating complicated synthetic reactions are limitless. Nanopores embedded in an insulating membrane fabricated by using a physical method has been demonstrated useful to examine biomolecules one by one, achieving single-molecule analysis.[88]

Besides the above applications, there are also tremendous opportunities for nanoporous materials in the following areas.[96] (1) high efficiency filtration and separation membranes. (2) catalytic membranes for chemical processes. (3) porous electrodes for fuel cells. (4) high efficiency thermal insulators. (5) electrode materials for batteries. (6) porous electronic substrates for high speed electronics.[88]

2.4. **NANOWIRE**

A nanowire is a nanostructure, with the diameter of the order of a nanometer (10^{-9} meters). Alternatively, nanowires can be defined as structures that have a thickness or diameter constrained to tens of nanometers or less and an unconstrained length. At these scales, quantum mechanical effects are important ð which coined the term "quantum wires". Many different

types of nanowires exist, including metallic (e.g., Ni, Pt, Au), semiconducting (e.g., Si, InP, GaN, ZnO, etc.), and insulating (e.g., SiO_2, TiO_2).

2.4.1. Applications of Nanowire

Nanowire sensors have been demonstrated that can detect the presence of many gases, including oxygen [22], hydrogen, NO_2, and ammonia [23], at very low concentrations. Nanowires also have been used to detect ultraviolet light [24], changes in pH [25], and the presence of low-density lipoprotein cholesterol [26].

In medicine, Nanowires are used for the production of nanoscale sensors for various purposes, one of which is in the detection of potential biomarkers of cancer. For example, nano-sized sensing wires that are laid across a microfluid channel can pick up molecular signatures of the particles and can relay the information instantaneously and these sensors can detect altered genes that are associated with cancer and ultimately have the potential to provide information on the location of the malignant genes [28].

In electronics, several semiconductor devices such as junction diodes, memory cells and switches [33], transistors, FETs, LEDs and inverter [34] etc have already been fabricated using nanowire junctions.

The huge surface area and the high conductivity along the length of nanowires are suitable for inorganicï organic solar cell [37].

2.4.2. Synthesis of Metal Oxide Semiconductor Nanowires

Various chemical, physical, and electrochemical deposition techniques have been reported to create oriented MOS (metal oxide semiconductor) nanowires. Methods such as catalytic growth via vapour-liquid-solid epitaxial (VSLE) mechanism, metal-organic chemical vapour deposition (MOCVD), pulsed laser deposition (PLD), chemical vapour deposition (CVD), hydrothermal synthesis, solution approaches and electrodeposition have been particularly successful in creating highly oriented arrays of anisotropic nanowires of ZnO.[100] In general, there are two philosophically distinct approaches for creating nanowires: top-down and bottom-up strategies. The top-down approach usually including etching and lithography in bulk materials to form functional devices, this approach has been successful in many venues. In the bottom-up

approach, functional nanostructures are assembled from well-defined chemically and/or physically synthesized building blocks.

Zinc oxide nanowires are commonly synthesized by a bottom-up approach.[101] CVD is a widely used route to produce high-purity, high-performance materials. In the CVD method, the precursor gases are first delivered into a reaction chamber at approximately ambient temperatures. In the reaction chamber a heated substrate or a wafer is used to expose to the volatile precursors, which react and decompose on the substrate surface to produce the desired solid phase. The by-products are removed by gas flow through the reaction chamber. Commonly, CVD is a generic name for a group of processes that involve depositing a solid material from a gaseous phase. CVD processes include: atmospheric pressure CVD (APCVD), low-pressure CVD (LPCVD), vapour phase epitaxy (VPE), chemical beam epitaxy (CBE), and metal-organic chemical vapour deposition (MOCVD).[102]

Another promising method to synthesize Zinc oxide nanowires is physical vapour deposition PVD. PVD is a technique quite similar to CVD, except that there is no chemical reaction happening during the deposition process. Variants of PVD include pulse laser deposition (PLD), and sputter deposition. These methods can produce high-quality, single crystalline wires. However, these processes require elevated temperatures of 450 ï 900 °C and often face other limitations of sample uniformly and substrate choice.[103]

Wang and co-workers have examined the synthesis, structure analysis,[104] and properties of nanoscale zinc oxide. They used solid-vapour thermal sublimation techniques to synthesize ZnO nanowires, nanobelts, nanorings, nanocages, and nanocombs. Zinc oxide nanowires and nanorods could be synthesized in many routes, such as vapour-liquid-solid (VLS) growth. In this technique, a metal catalyst, such as Au or Sn, was chosen and serves as the site for adsorbing the incoming molecules (Zn complexes). A liquid alloy droplet composed of the metal catalyst is formed, followed by addition of the gaseous precursor to form an AuZn alloy. The metal liquid droplet serves as a preferential site for absorption of gas-phase reactant. Nanowire growth begins after the liquid becomes supersaturated in reactant materials and continues as long as the catalyst alloy remains in a liquid state and the reactant is available. The growth terminates when the temperature is below the eutectic temperature of the catalyst alloy or the reactant is no longer available. As a result, the nanowires obtained from the VLS process typically have a solid

catalyst nanoparticle at the ends with sizes comparable to diameters of the connected nanowires.

In contrast to gas-phase technologies, solution approaches are appealing because of the low growth temperature (< 350 °C), potential for scaling up, and straight-forward methods of producing high-density arrays. Chemical bath deposition (CBD) is one of the useful solution methods for the preparation of compound semiconductors from aqueous solution, with advantages such as low processing temperature, allowing growth upon a variety of substrates, and easy adaptation to large area processing at low fabrication cost.[105] In chemical bath deposition technique, deposition of metal oxide semiconducting thin films occurs due to substrate maintained in contact with chemical bath containing metal ions. The film formation on substrate takes place when the ionic product exceeds the solubility product. The CBD method is based on the controlled precipitation of the material to be prepared, so as to produce a film upon the substrate surface. Although the precipitation can be controlled by adjusting the experimental conditions (chemical composition and process temperature), nucleation in the solution and on the reactor wall cannot be avoided. Hence only a small amount of the reagents in the solutions are used for film growth and a larger amount of material produces colloidal particles in the solution. Only 2% of the reagents in the solution is used during CBD growth on the substrate.[106] M. Izaki[107] has prepared highly (0001)-oriented ZnO films by UV light-assisted CBD from an aqueous solution containing hydrated zinc nitrate and dimethylamineborane (DMAB). A recent report has shown that the CBD method can be used to synthesize ZnO films and nanorod arrays on different substrates.[108] Yang et al. have prepared ZnO nanowire with CBD using silicon substrate and found the average diameter of the nanowire to be 125nm.[109]

Hydrothermal syntheses are another convenient method to synthesis semiconductor nanowires. For example ZnO nanowires can be obtained by the hydrolysis of zinc nitrate in water in the presence of an amine. The zinc(II) is solvated by water, and exists as several monomeric hydroxyl species, such as $Zn(OH)^{+}(aq)$, $Zn(OH)_2(aq)$, and $Zn(OH)_4^{2-}(aq)$. The stability of these complexes is dependent on the pH and temperature of the solution. Solid ZnO nuclei are formed by the dehydration of these hydroxyl species, shown in equation 1. Additives to the solution mixture, often amines, have a strong effect on the morphology of the resulting crystal.[110]

$$Zn(OH)_{2\,(aq)} \text{ Ÿ } ZnO_{(s)} + H_2O_{(aq)} \qquad (1)$$

Finally, electrodeposition has three main attributes that make it a promising technique for fabrication of nanowires. First, it can be used to grow functional materials through complex 2D or 3D templates; second, it can be performed at temperatures near room temperature from water-based electrolyte solutions; and finally, it can be scaled down to the deposition of a few atoms as well as up to larger dimensions. Electrodeposition within anodic alumina membrane templates is a bottom-up synthesis route which has been used with a great deal of success by numerous groups to synthesize metal and semiconductor nanostructures.[111] In a typical synthesis, a piece of anodic aluminum oxide (AAO) membrane with highly ordered nanopores is used as growth template. The dimensions of the nanopores can be varied over a large length scale. The backside of the membrane is homogeneously coated by a conducting layer, such as silver or GaN.[111] An aqueous solution with a certain concentration of metal cations is applied as the electrolyte, and the conducting layer acts as the cathode lead. In the electrodeposition process, the metal ions are reduced and the metal nanowires grow in the pores of the template. Meanwhile, a pure metal wire is used as the anode; during the electrodeposition process, the sacrificial anode is oxidized and therefore compensates the loss of metal cations in the electrolyte. The length of the nanostructures can be controlled by adjusting the amount of metal deposited. After the electrodeposition process, free-standing nanowires can be obtained through the removal of conducting layer and the dissolution of alumina membrane. CaO reviewed the growth of nanostructures using membranes as templates by using electrodeposition methods, metallic nanowires, such as Ni and Bi, conducting polymers, such as polyaniline (PANI), and oxides, such as ZnO, could be successfully synthesized with high efficiency.[112]

CHAPTER THREE

3.0 EXPERIMENTAL

3.1 Materials and Method

In this work, chemical bath deposition method (CBD) was used for the growth of ZnO nanowire. CBD method was employed based on the following reasons;

(a) The growth temperature can be as low as $50^{o}C$.
(b) With such low temperature, much cheaper substrates such as plastic and glass can be used.
(c) Less sophisticated equipments are required.
(d) The cost of chemicals/reagents is relatively low.
(e) It is environmentally friendly.
(f) The properties of the deposited material can be varied and controlled by proper optimization of chemical baths and deposition conditions.

3.1.1. Equipment/Instruments

The following equipments were used during the investigation.

Digital-Temperature regulation oven (Gallenkamp)

Glass beakers (pyrex)

$1dm^3$ -Volumetric flask (pyrex)

Electronic weighing balance (B. Brian)

pH meter (jenway 3510)

Spectrophotometer (UNICO-UV-Vis-NIR 2120 PC).

SEM (Carl Zeiss EVO MA/10)

Powder X-ray diffraction (Rigaku Rotaflex RU-200 rotating anode XRD)

Stop watch (quatz)

Syringe

Pipette

Microscopic glass slides

3.1.2. CHEMICALS

Hexamine (99.9% purity) from Bendosen

Zinc nitrate hexahydrate (99.9% purity) from fluka

Zinc acetate dihydrate (98% purity) from Aldrich

Ethanol (98% purity, $\rho = 0.788\ gcm^{-3}$) from Aldrich

Ammonia (98% purity, $\rho = 0.9\ gcm^{-3}$) from May & Baker Ltd.

Distilled water.

All chemicals were analytical grade reagents and were used without further purification. All the aqueous solutions were prepared using distilled water.

The synthesis of ZnO nanowire combines substrate pretreatment and CBD growth as described below.

Substrate Preparation

Prior to deposition of ZnO nanowire, glass micro slides were chemically degreased by treatment with dilute HCl for 24h, later cleaned in detergent/cold water and rinsed with distilled water and allowed to drip dry in air.

Substrate Pretreatment

Equal volumes (10 ml) each of zinc acetate dihydrate [$Zn(OOCCH_3)_2.2H_2O$] (0.05M) and ethanol (0.05M) were mixed in a 50 ml beaker. This solution was coated on glass substrates by spin coater (Laurell WS-400-STFW-FULL) at rate of 2000rmp for 30s. The thickness of the zinc acetate layer can be controlled by the number of spin coating runs and show good reproducibility. Here, substrates were spin coated twice. The coated substrates were dried at room temperature and annealed at 150^o for 30min. All the substrates were pretreated twice before the final growth of ZnO nanowire.

Chemical Bath Deposition (CBD) Growth

For CBD growth process, the aqueous solution of zinc nitrate hexahydrate and hexamine were first prepared. The concentrations of both were fixed at 0.1M. Aqueous solutions of zinc nitrate hexahydrate (20 ml) and hexamine (20 ml) were mixed together in 50 ml beaker. Aqueous ammonia (0.1M) was added to the solution to vary the pH. The amount added depends on the targeted pH. In this work, 4-6ml of aqueous ammonia was added to raise the pH to 9.00 and 10.0 respectively. The pH of the original growth solution was 8.1.

The original growth solution (pH of 8.1) was transparent and contains white dispersed precipitates of $Zn(OH)_2$.The bath solutions at pH 9.0 and 10.0 dissolved and appeared white turbid in nature (milky).

The pretreated glass slides (substrates) were immersed into the three different bath solutions and tilted against the wall of the beaker. The beakers containing the bath solutions and the substrates were put in the oven for 2h at a constant temperature of 93^{o}C. After the growth, the substrates were removed from the solutions, rinsed with distilled water and then dried at room temperature.

White dense, uniform deposition was observed on the samples grown at the pH of 8.1. Whereas, less dense milky deposition was observed on the samples grown at pH of 9.0 and slightly transparent white deposition was observed on samples grown at pH of 10.0

Post Growth Annealing

A post growth thermal annealing was performed for the substrates (samples) from the three different pH solutions (8.1, 9.0 & 10.0) at 100^{o}C, 150 ^{o}C and 200 ^{o}C respectively for 1h and then quenched to room temperature by removal from the oven.

Table1. SAMPLE IDENTIFICATION

SAMPLE	GROWTH pH	ANNEALING TEMPERATURE (^{O}C)
W8100	8.1	100
W8150	8.1	150
W8200	8.1	200
W9100	9.0	100
W9150	9.0	150
W9200	9.0	200
W10100	10.0	100
W10150	10.0	150
W10200	10.0	200

CHAPTER FOUR

RESULTS AND DISCUSSION

4.1. MORPHOLOGICAL ANALYSIS (SEM)

The results of morphological analysis (surface structure) of the deposited ZnO nanowire which was carried out using scanning electron microscope as shown in Fig. 2 to Fig. 9 at varying PH levels.

The nanowires grown at the normal pH of the bath solution (8.1) possesses hexagonal shape and their diameters were measured at different angles such as 90^0 and 132.3^0 across the breadth of the nanowire between two points (Pa1 & PaR1) and was found to be between 170.3 and 481nm as shown in Fig. 3-4 below:

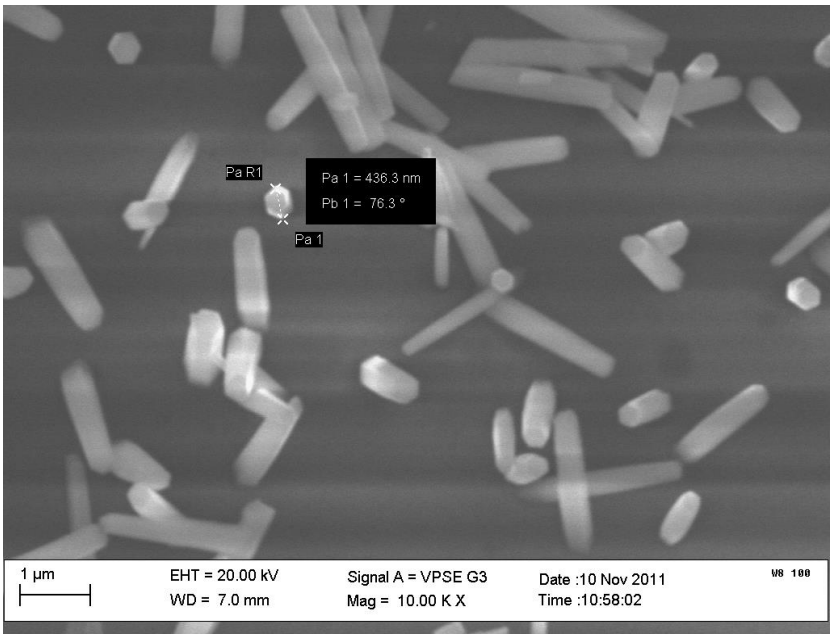

Fig.2. SEM of W8100 grown at pH 8.1 and annealed at 100 ^{o}C

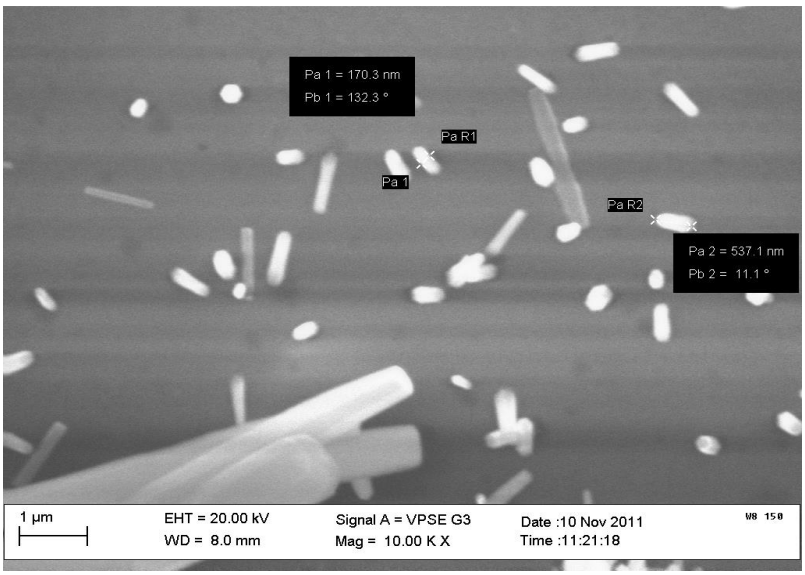

Fig.3. SEM of W8150 grown at pH 8.1 and annealed at 150 ^{o}C

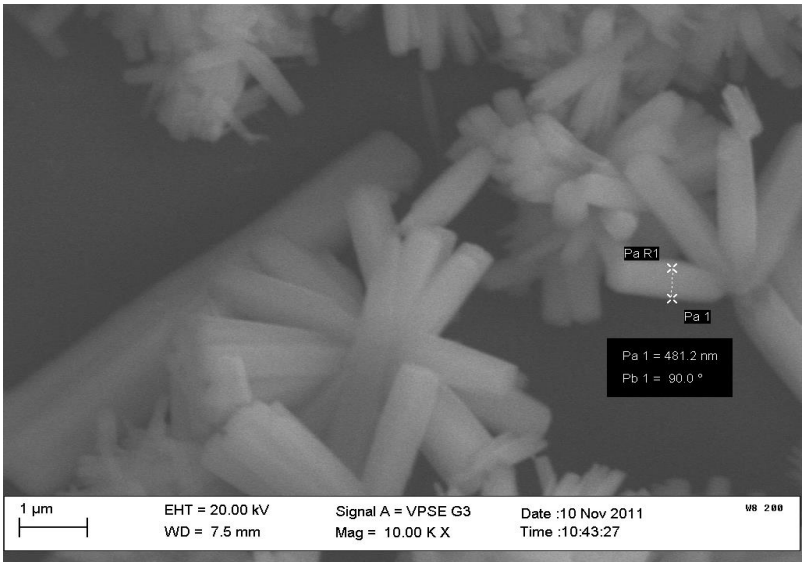

Fig.4. SEM of W8200 grown at pH 8.1 and annealed at 200^{o}C

However, the samples grown at pH of 9.0 and 10.0 were observed to be nanostructures with tapered flower -like shape as shown in Fig. 5-9 below. This shape transformation might be due to the competition between growth and erosion. As is well known, the hexagonal wurtzite ZnO crystal is a typical polar crystal with a dipole moment in the direction of c-axis, so the (0001) crystal plane represents the polarity and is metastable, but the side planes are non-polar and relatively more stable. The polar top planes are able to attract OH^-, which could erode the planes in the solution according to the following equation;

$ZnO + OH^- \ddot{Y} ZnO_2^{2-} + H_2O$ 2

For the original growth solution, the OH^- in the solution is only enough to grow the nanowires. After the aqueous ammonia was added , more and more OH^- were formed when the solution was heated so that the total amount of OH^- was not totally consumed during the growth. Then the rest of the OH^- in the solution also took part in the erosion reaction at the same time. The relative erosion process will become more and more intensive as the pH is increased. However, during the CBD growth process, the growth speed will be faster than that of erosion. As a result of the competition between growth and erosion, the top of ZnO nanowires become tapered at pH between 9.0 and 10.0.

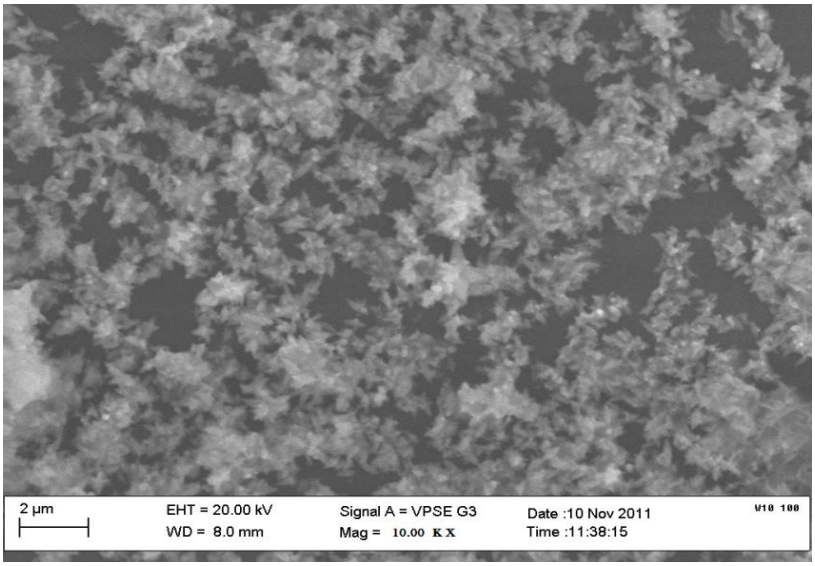

Fig.5. SEM of W9100 grown at pH 9.0 and annealed at 100 ^{o}C

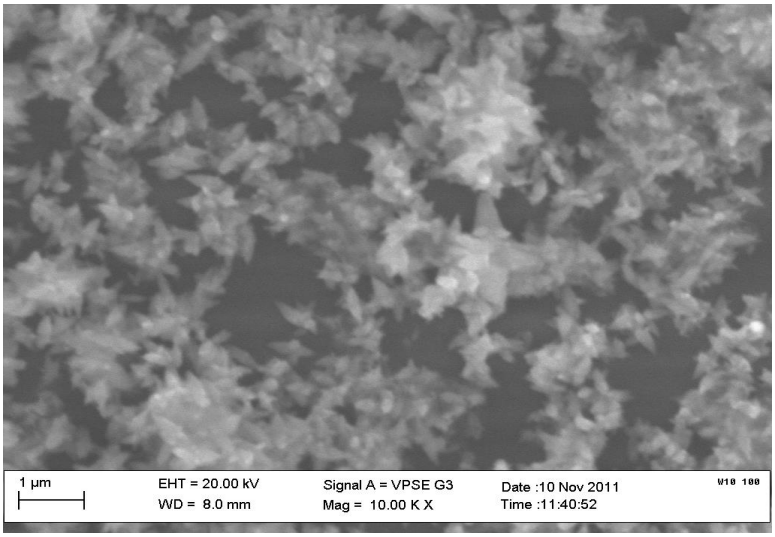

Fig.6. SEM of W9150 grown at pH 9.0 and annealed at 150 ^{o}C

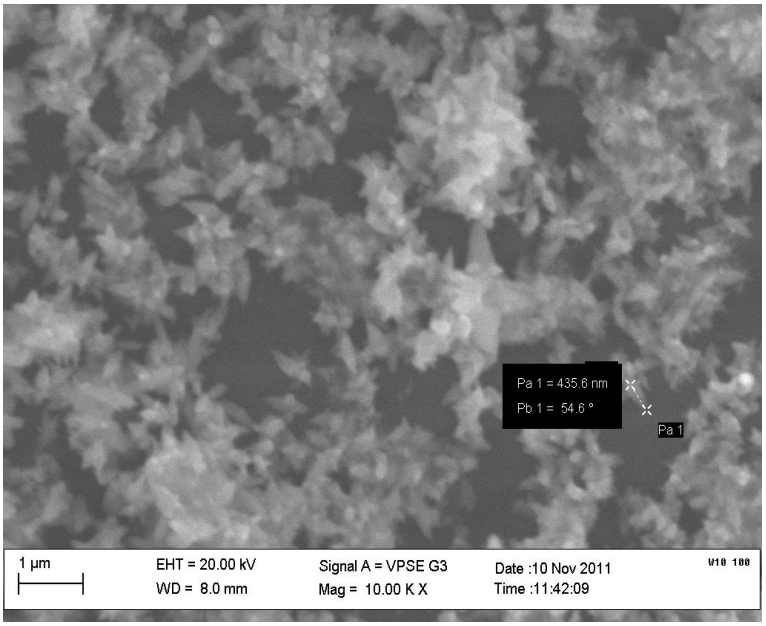

Fig.7. SEM of W9200 grown at pH 9.0 and annealed at 200 ^{o}C

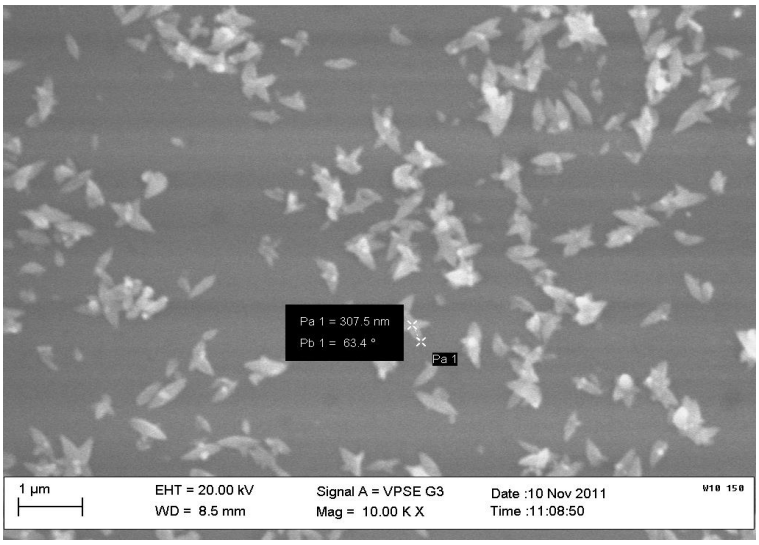

Fig.8. SEM of W10150 grown at pH 10.0 and annealed at150 ^{o}C

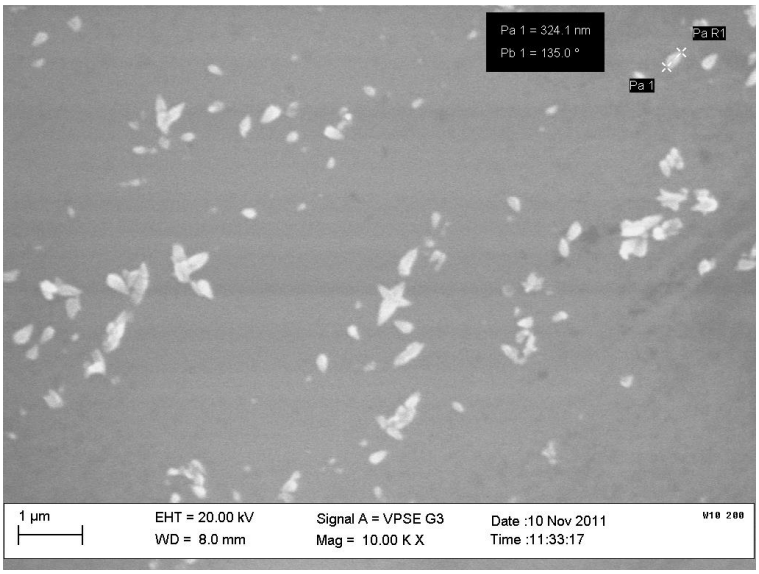

Fig.9. SEM of W10200 grown at pH 10.0 and annealed at 200^{o}C

The SEM micrographs shows that as the growth pH is increased from original pH of the solution, the morphology or shape of the nanowire changes from hexagonal structure to tapered flower-like structure. Therefore, the original pH, 8.1 in the solution is the optimized value to form ZnO nanowires with the top surface of hexagonal shape.

4.2. **X-RAY DIFFRACTION ANALYSIS**

The XRD analysis was carried out for samples grown at pH of 8.1. In order to study the crystalline nature of the deposited nanowires, the XRD patterns were recorded in the 2ɗ ranging from 10 - 70° with CuK_2 (ɔ = 1.5406 Å) and the intensity was plotted against 2ɗ**.**

The XRD diffraction pattern and peak related values of annealed nanowires are shown in fig.10. Correlating the angular diffraction in the 2ɗ range with ZnO compound phase (fig. 11), three peaks at a 2ɗ value of 33.77, 44.82 and 53.63 for sample W8100 matched, two peaks at a 2ɗ value of 44.88 and 66.40 for sample W8150 matched and three peaks at a 2ɗ value of 31.82, 56.68 and 67.96 matched for sample W8200.

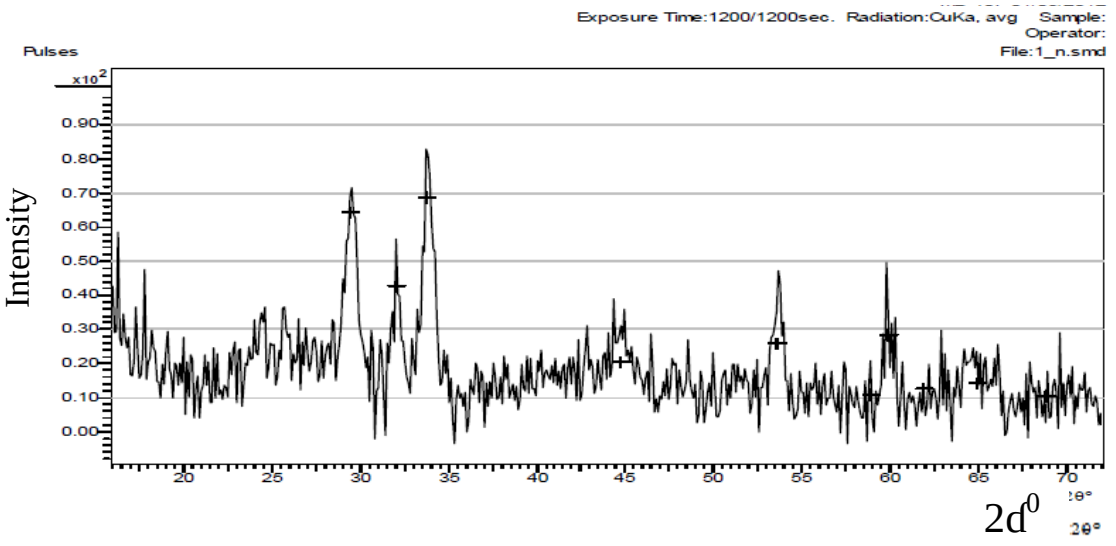

2θ°	d	I int	I max	I rel	I corr	FWHM
20.11	3.03313	1317	63.0	93.2	97.1	0.28061
32.02	2.79508	970	41.7	61.6	62.6	0.28941
33.77	2.65379	1413	67.7	100.0	100.0	0.28912
44.82	2.02230	404	19.4	28.6	26.7	0.27997
53.63	1.70895	519	24.8	36.7	33.2	0.27168
58.90	1.56791	199	9.5	14.1	12.6	0.28105
59.89	1.54440	564	27.0	39.9	35.6	0.283
61.87	1.49955	239	11.5	16.9	15.0	0.28115
64.91	1.43644	272	13.0	19.2	17.0	0.27828
66.77	1.39900	193	9.2	13.7	12.0	0.26039

Fig.10. X-Ray Diffraction pattern of W8100

36-1451 Quality: Quality Data

Zn O
Zinc Oxide
Zincite, Syn

Rad:CuKa1	Lambda:1.540598	Filter:Monochromator crystal used		d sp:Diffractometer
Cutoff:	Int:Diffractometer	I/Icor:		
Ref:McMurdie, H., Morris, M., Evans, E.,Paretzkin, B., Wong-Ng, W., Ettlinger, L.,Hubbard, C.1. Bragg, W.2. Abrahams, S., Berr				
Sys:Hexagonal		S.G.:P63mc		
a:3.24982±9E-5	b:	c:5.20661±0.00015		
α:	β:	γ:	Z:2	mp
Ref2				
Dx:	Dm:5.675	SS/FOM: F27=130.8(0.0071,29)		Volume[CD]:47.62
εα:	ηωβ:2.013	εγ:2.029	Sign:+	2V:
Ref3				

Color:Colorless

The sample was obtained from the New Jersey Zinc Co., Bethlehem, PA, USA. The structure was determined by Bragg (1) and refined by Abrahams, Bernstein (2). A high pressure cubic NaCl-type of ZnO is reported by Bates et al. (3) and a cubic, sphalerite type is reported by Radczewski, Schicht (4). The approximate temperature of data collection was 26 C. To replace 5-664 (5). References to other early patterns may be found in reference (5).

18 reflections in pattern. Wavelength 1.5406 was used to calculate the diffraction angles.

2 θ	Int.	h k l	2 θ	Int.	h k l	2 θ	Int.	h k l	2 θ	Int.	h k l
26.2678	10		58.7649	90							
28.6811	30		62.7280	60							
30.9169	20		69.5831	60							
33.6664	100		82.3523	10							
36.4959	50		85.0173	10							
39.1345	20		89.9336	10							
41.9891	30		98.0850	20							
44.6002	10		115.6625	20							
47.5691	50										
54.5823	50										

Fig.11. Compound phase of W8100.

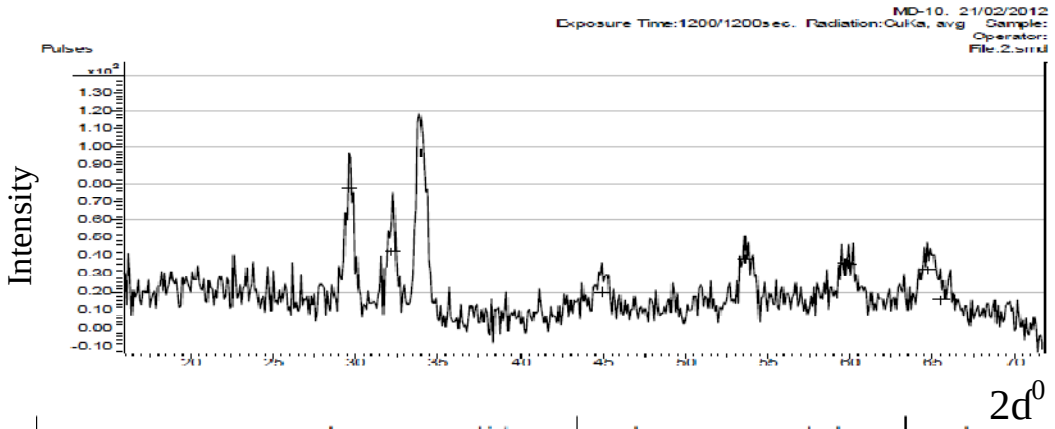

2θ°	d	I int	I max	I rel	I corr	FWHM
29.55	3.02248	2874	78.6	56.8	59.4	0.50496
32.14	2.78467	2140	46.8	42.3	43.0	0.6314
33.91	2.64385	5057	101.9	100.0	100.0	0.68424
44.00	2.01943	1241	25.1	24.5	22.9	0.6604
53.61	1.70932	1435	39.2	28.4	25.7	0.47297
59.70	1.54875	1343	36.7	26.6	23.7	0.49359
59.90	1.54411	1318	36.1	26.1	23.3	0.49411
64.72	1.44027	1570	23.0	31.2	27.0	0.89159
65.52	1.42456	402	7.4	0.0	7.0	0.72051
66.40	1.40780	453	7.7	9.0	7.9	0.78728

Fig.12. X-Ray Diffraction pattern of W8150

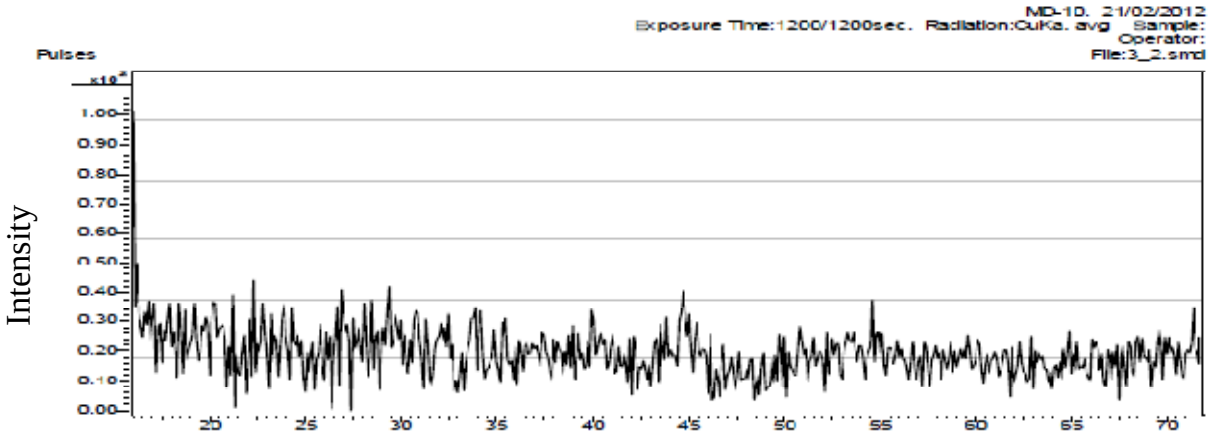

2ɗ	d values	I int.	I max.	I rel.	I corr.	FWH.M
19.36	4.58447	111	5.3	20.4	24.7	0.279
19.70	4.50548	75	3.6	13.8	16.5	0.279
20.11	4.41629	96	4.6	17.6	20.9	0.279
20.15	4.40698	127	6.1	23.2	27.4	0.279
21.03	4.22342	140	6.7	25.7	29.5	0.279
21.39	4.15464	64	3.1	11.7	13.4	0.279
21.66	4.10314	239	11.4	43.7	49.4	0.279
21.96	4.04793	249	11.9	45.5	51.1	0.279
22.27	3.99161	422	20.2	77.3	86.0	0.279
22.61	3.93234	324	15.5	59.3	65.5	0.279
22.70	3.91764	364	17.4	66.6	73.3	0.279
22.94	3.87654	465	22.3	85.1	93.2	0.279
23.91	3.72182	386	18.5	70.6	75.7	0.279
24.85	3.58251	70	3.3	12.7	13.4	0.279
24.91	3.57468	92	4.4	16.9	17.7	0.279
25.00	3.56141	416	19.9	76.1	79.9	0.279
25.27	3.52400	188	9.0	34.4	35.9	0.279
25.62	3.47751	308	14.7	56.3	58.5	0.285
25.86	3.44474	241	11.6	44.2	45.6	0.288
26.16	3.40637	229	11.0	41.9	43.1	0.288
26.60	3.35088	479	22.9	87.6	89.5	0.288
26.88	3.31677	219	10.5	40.1	40.8	0.288
27.12	3.28796	210	10.1	38.5	39.0	0.288
27.37	3.25884	145	6.9	26.5	26.7	0.289
27.53	3.23975	222	10.6	40.6	40.9	0.289
27.54	3.23874	130	6.2	23.9	24.0	0.289
27.95	3.19157	291	13.9	53.3	53.4	0.289
28.04	3.18250	546	26.2	100.0	100.0	0.289
28.57	3.12404	308	14.8	56.4	56.0	0.289
29.20	3.05857	279	13.4	51.1	50.3	0.289
29.72	3.00610	496	23.8	90.8	88.9	0.289

30.39	2.94095	134	6.4	24.6	23.8	0.288
30.97	2.88693	129	6.2	23.6	22.7	0.288
31.82	2.81245	230	11.0	42.2	40.3	0.288
32.24	2.77618	212	10.1	38.8	36.9	0.288
32.59	2.74736	105	5.0	19.3	18.3	0.288
34.12	2.62747	35	1.7	6.5	6.1	0.288
40.01	2.25349	126	6.0	23.0	20.6	0.284
51.94	1.76028	58	2.8	10.6	9.1	0.272
52.20	1.75216	45	2.2	8.3	7.1	0.272
53.25	1.72018	66	3.2	12.1	10.3	0.271
53.53	1.71172	103	4.9	18.8	16.0	0.270
53.87	1.70178	87	4.2	15.9	13.5	0.270
54.24	1.69121	44	2.1	8.1	6.9	0.270
54.56	1.68194	86	4.1	15.8	13.4	0.270
54.79	1.67545	92	4.4	16.9	14.3	0.270
55.58	1.65333	58	2.8	10.6	9.0	0.270
55.81	1.64707	27	1.3	4.9	4.2	0.270
56.22	1.63614	40	1.9	7.3	6.2	0.271
56.68	1.62391	71	3.4	13.0	11.0	0.272
56.91	1.61786	92	4.4	16.9	14.2	0.272
57.40	1.60516	108	5.2	19.8	16.7	0.274
57.75	1.59644	61	2.9	11.1	9.4	0.275
58.00	1.59019	80	3.8	14.6	12.3	0.277
58.29	1.58294	129	6.2	23.6	19.8	0.278
58.78	1.57095	118	5.7	21.6	18.1	0.280
58.99	1.56586	134	6.4	24.6	20.6	0.280
59.29	1.55844	97	4.6	17.7	14.9	0.281
59.58	1.55174	175	8.4	32.1	26.9	0.282
59.97	1.54246	118	5.6	21.5	18.0	0.282
60.42	1.53200	110	5.2	20.1	16.8	0.283
60.83	1.52265	69	3.3	12.6	10.6	0.283
61.57	1.50623	111	5.3	20.3	16.9	0.282
61.82	1.50066	96	4.6	17.5	14.6	0.281
62.16	1.49333	110	5.3	20.1	16.8	0.281
62.55	1.48491	100	4.8	18.3	15.2	0.280
62.89	1.47779	74	3.5	13.5	11.2	0.279
63.23	1.47048	78	3.7	14.3	11.9	0.279
63.39	1.46729	106	5.1	19.4	16.1	0.279
64.15	1.45162	29	1.4	5.3	4.4	0.278
64.39	1.44686	109	5.2	19.9	16.6	0.278
64.74	1.43992	89	4.3	16.3	13.5	0.278
65.03	1.43416	80	3.8	14.6	12.1	0.278
65.43	1.42628	101	4.8	18.4	15.3	0.279
65.78	1.41956	68	3.3	12.5	10.4	0.279
66.10	1.41343	58	2.8	10.5	8.7	0.280

66.34	1.40894	82	3.9	15.0	12.4	0.280
66.57	1.40474	99	4.7	18.1	15.0	0.281
66.85	1.39951	64	3.1	11.8	9.7	0.281
67.33	1.39071	35	1.7	6.4	5.3	0.283
67.75	1.38303	57	2.7	10.4	8.6	0.283
67.96	1.37922	70	3.3	12.7	10.5	0.283
68.20	1.37494	42	2.0	7.7	6.3	0.282
68.40	1.37146	46	2.2	8.4	7.0	0.280
68.75	1.36535	62	3.0	11.4	9.4	0.279
69.83	1.34694	47	2.3	8.7	7.1	0.279
70.09	1.34249	35	1.7	6.3	5.2	0.279

Fig.13. X-Ray Diffraction pattern of W8200

The average crystallite sizes of the nanowires were deduced by the inverse proportional relation of the full width at half maximum (FWHM), as predicted by Debye-Scherrerôs equation:

$$D = 0.9\lambda/\beta\cos\theta \quad \text{.....11}$$

Where D is the crystalline size, λ is the X-ray wavelength used (1.5406 Å), β is the full width at half maximum (FWHM) intensity, and θ is the Braggôs angle (diffraction angle).

For W8100, the three peaks at a 2θ value that matched with their corresponding FWHM are 33.77, 44.82, 53.63 at 0.28912, 0.27997 and 0.27168 respectively.

At θ = 33.77,

$$D = 0.9\lambda/\beta\cos\theta = \frac{0.9 \times 1.5406}{0.28912 \times \cos(\frac{33.77}{2})} = 5.0127 \text{ Å} = 0.50127 \text{ nm}$$

At θ = 44.82,

$$D = 0.9\lambda/\beta\cos\theta = \frac{0.9 \times 1.5406}{0.27997 \times \cos(\frac{44.82}{2})} = 5.357 \text{ Å} = 0.5357 \text{ nm}$$

At θ = 53.63,

$$D = 0.9\lambda/\beta\cos\theta = \frac{0.9 \times 1.5406}{0.27168 \times \cos(\frac{53.63}{2})} = 5.720 \text{ Å} = 0.572 \text{ nm}$$

Average crystallite size for W8100 = $\frac{0.5012 + 0.5357 + 0.572}{3} = 0.536$ nm

The average crystallite sizes for W8150 and W8200 were similarly deduced and the results are shown in the table below.

Table. 2. Nanowire crystallite size

Sample	Annealing temperature (^{0}C)	Average crystallite size (nm)
W8100	100	0.536

W8150	150	0.541
W8200	200	0.557

The result from the table shows that the average crystallite size increases with increase in annealing temperature.

The X-Ray Diffraction analysis shows that ZnO nanowire has a hexagonal crystallite structure with lattice parameters; a = 0.3296, b = 0.3296 and c = 0.52065 (a = b Í c) as shown in Fig.11 above which agrees with the condition for a lattice structure to be hexagonal.

The interpanar spacing (d) which is the distance between the lattice structures on a plane were calculated for sample grown at pH 8.1 using Braggôs law for confirmation as shown below.

$d = \frac{\square\square}{\square\square\square\square}$ é 3

where, d = interpanar spacing, n = 1 for simple lattice structure, λ = X-ray wavelength used (1.5406 Å), ɗ = Braggôs angle (diffraction angle).

Table 3. Nanowire interplanar spacing

Braggôs angle(ɗ)	d- observed	d- calculated
16.89	2.653	2.652
22.41	2.022	2.020
26.82	1.708	1.707

The interplanar spacing (d- observed) from the table above is the interplanar spacing observed by the diffractometer and d- calculated is the interplanar spacing calculated for confirmation. The results from the table above show that there is no significant difference between the d- observed and d- calculated.

4.3. OPTICAL ANALYSIS

The optical properties of ZnO nanowires grown at pH of 8.1 and 9.0 were characterized using (UNICO-UV-Vis-NIR 2120 PC) spectrophotometer in the range of 172.8-1100 nm.

The plot of absorbance versus wavelength as shown in Fig. 14-21 shows that ZnO nanowire has high absorbance in the ultraviolet region (175.85nm).

However, the absorbance decreases gradually in the visible with gradual increment to infrared region. Transmittance, T is in contrast to the absorbance of the nanowire as it decreases with increases in absorbance.

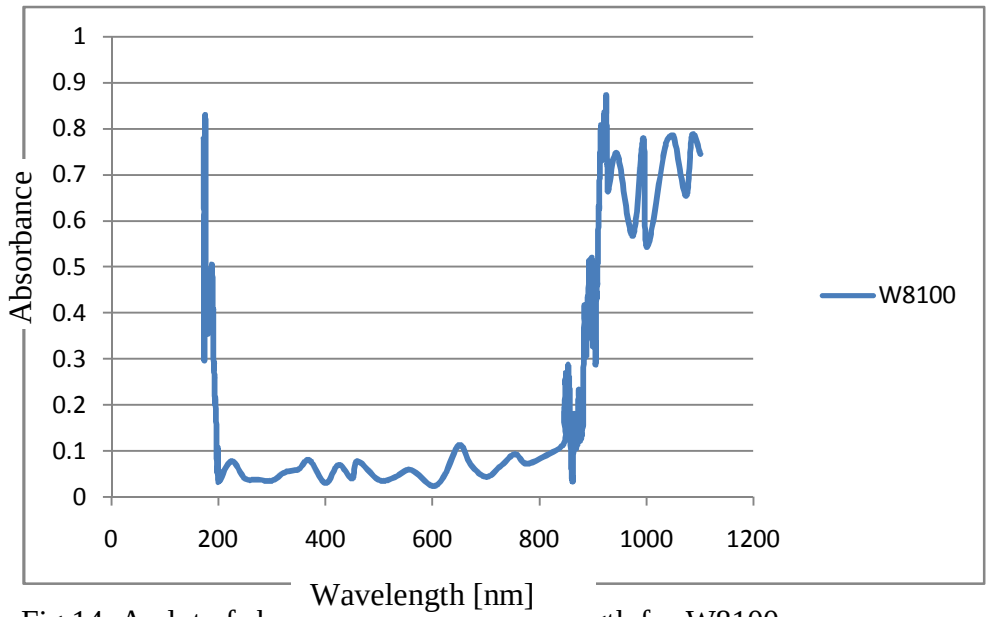

Fig.14. A plot of absorbance versus wavelength for W8100.

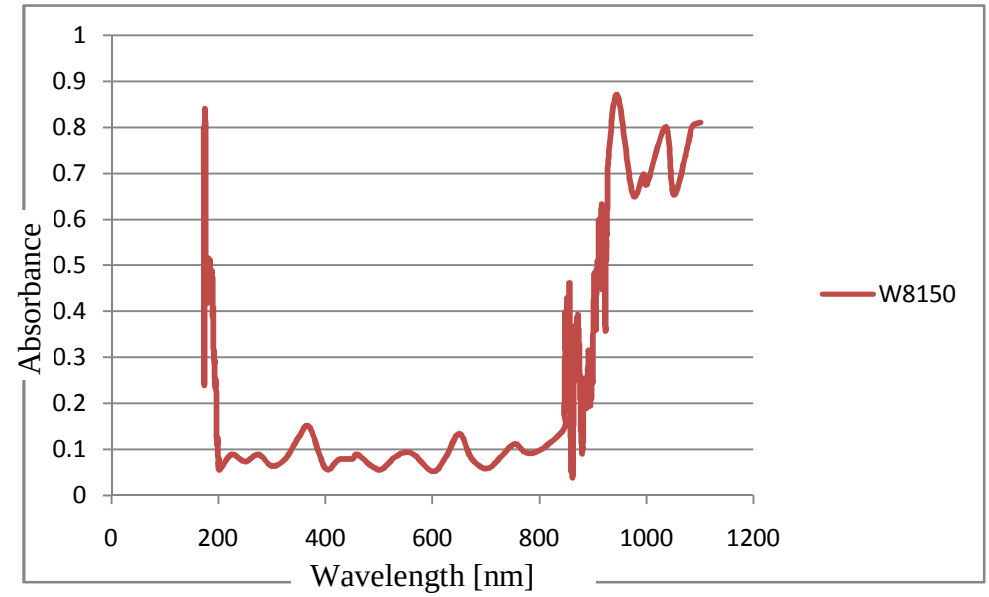

Fig.15. A plot of absorbance versus wavelength for W8150.

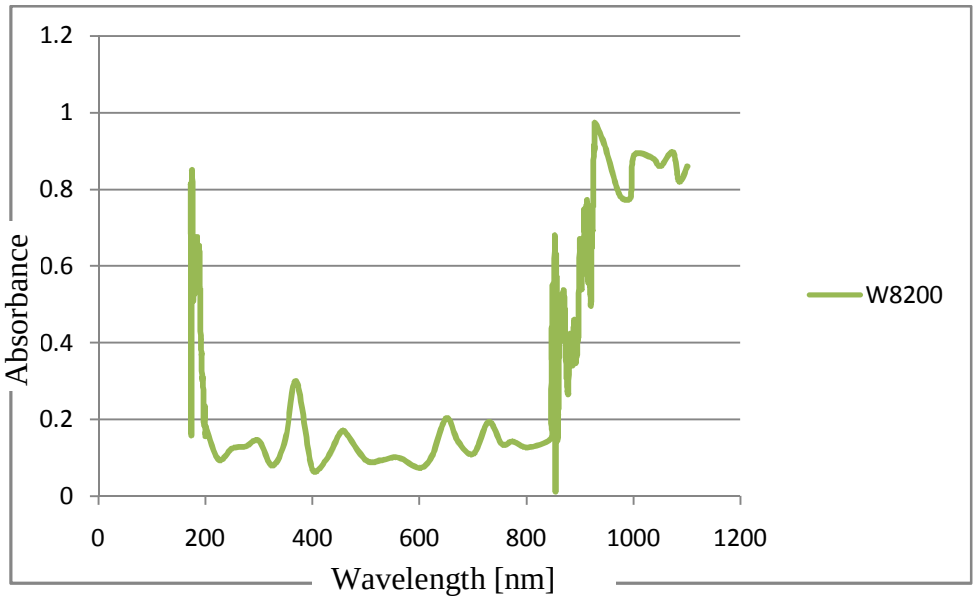

Fig.16. A plot of absorbance versus wavelength for W8200.

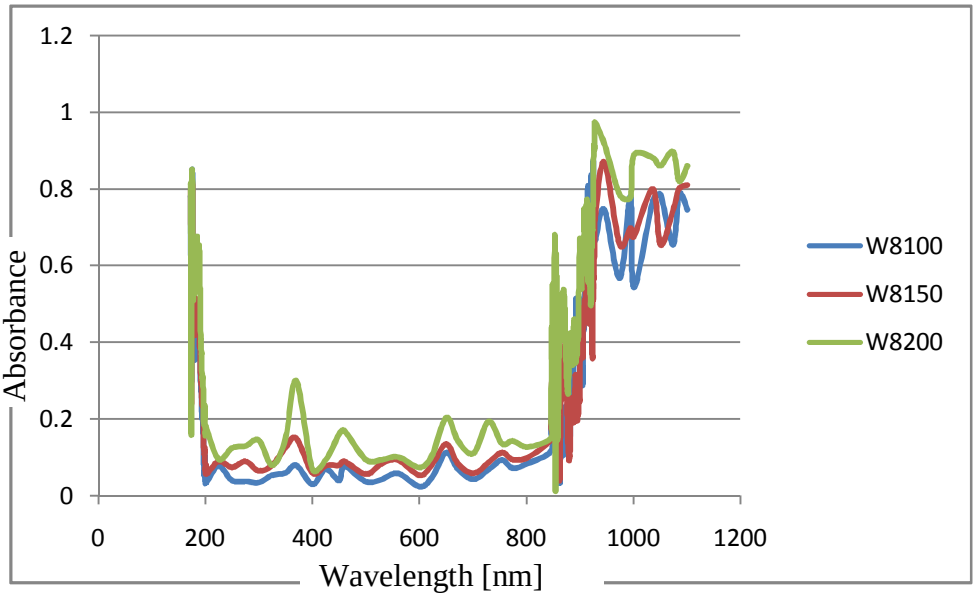

Fig.17. A correlation plot of absorbance versus wavelength for W8100,W8150 &W8200.

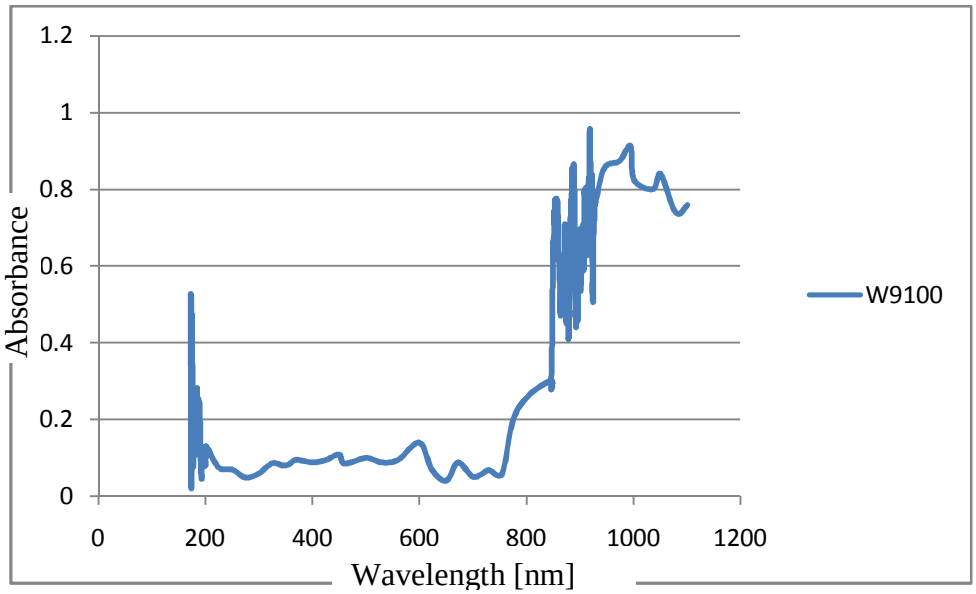

Fig.18. A plot of absorbance versus wavelength for W9100.

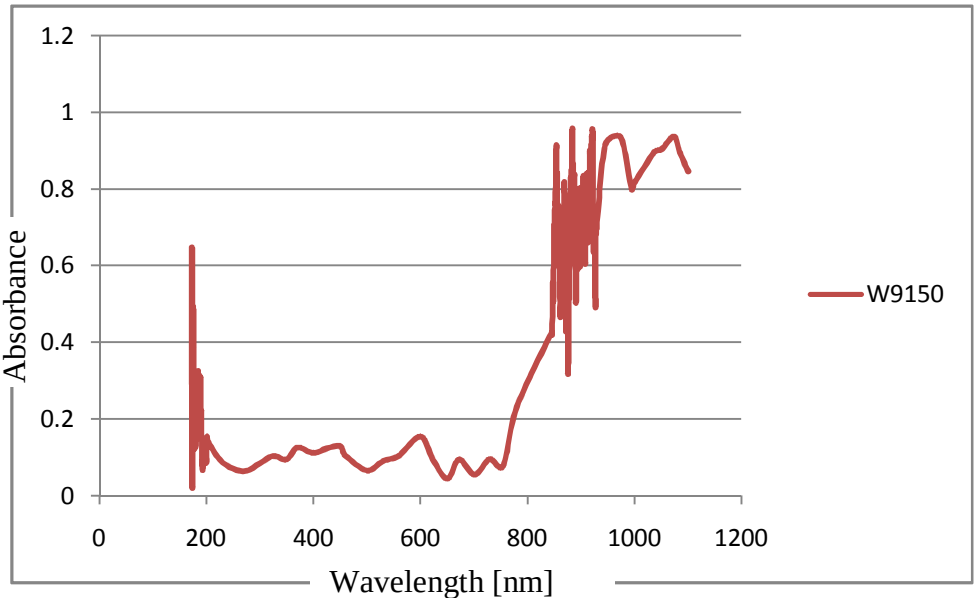

Fig.19. A plot of absorbance versus wavelength for W9150.

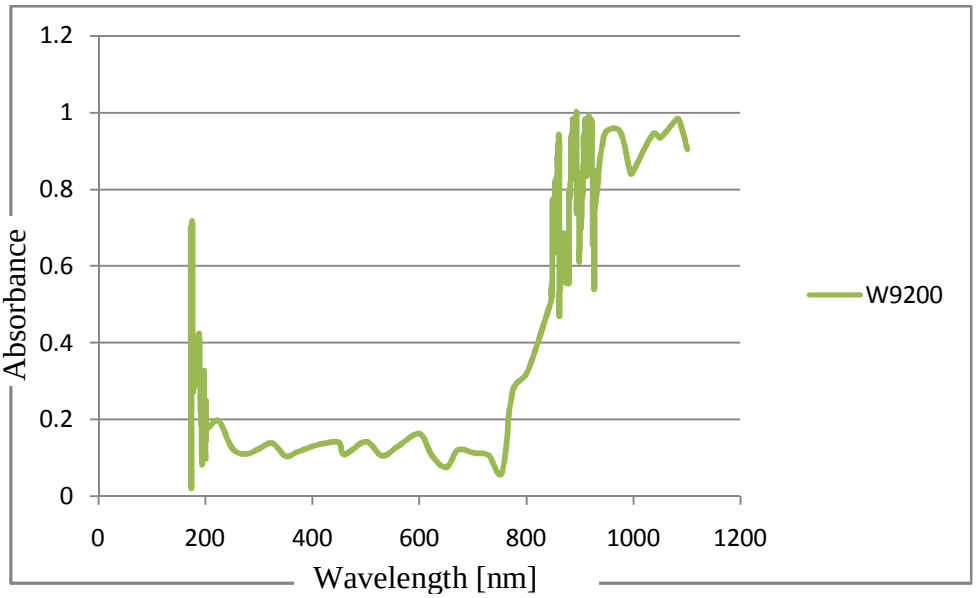

Fig.20. A plot of absorbance versus wavelength for W9200

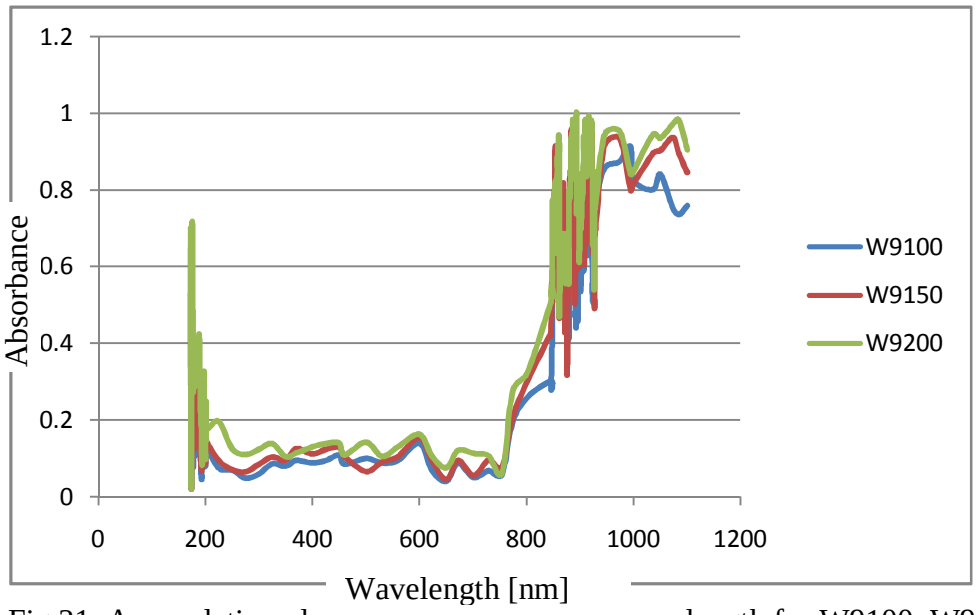

Fig.21. A correlation plot of absorbance versus wavelength for W9100, W9150 & W9200.

The correlation plot of absorbance versus wavelength in Fig. 17 & 21 showed a gradual increment in absorbance with increase in annealing temperature. At pH of 8.1, the absorbance were 0.82, 0.84 and 0.85 at 100^{o}C, 150^{o}C and 200^{o}C respectively while at pH of 9.0, the absorbance were 0.46, 0.64 and 0.71 at 100^{o}C, 150^{o}C and 200^{o}C respectively.

Its high absorbance in the ultraviolet region suggest that it can be use as solar harvester for trapping solar energy for photovoltaic panel which is capable of converting sunlight radiation directly to electricity for commercial or industrial purpose.

4.4. **COMPOSITIONAL ANALYSIS (EDX)**

The compositional study of the deposited ZnO nanowire was carried out by energy dispersive X-ray (EDX) at a potential difference of 14KV. The spectra reveal peaks, which contain both elemental compositions of glass substrate and the deposited nanowire. Each element has a unique atomic structure and binding energy. At rest, an atom within the sample contains ground state (or unexcited) electrons in discrete energy levels or electron shells bound to the nucleus. The incident beam excites an electron in an inner shell, ejecting it from the shell while creating an electron hole where the electron was. An electron from an outer, higher-energy shell then fills the hole, and the difference in energy between the higher-energy shell and the lower energy shell releases in the form of an X-ray. The number and energy of the X-rays emitted from a specimen is a characteristic of an element allowing unique sets of peaks on its X-ray spectrum.

The spectra were the same for all the samples. Shown in Fig. 22-23 are EDX result of sample W8100 and W9100.

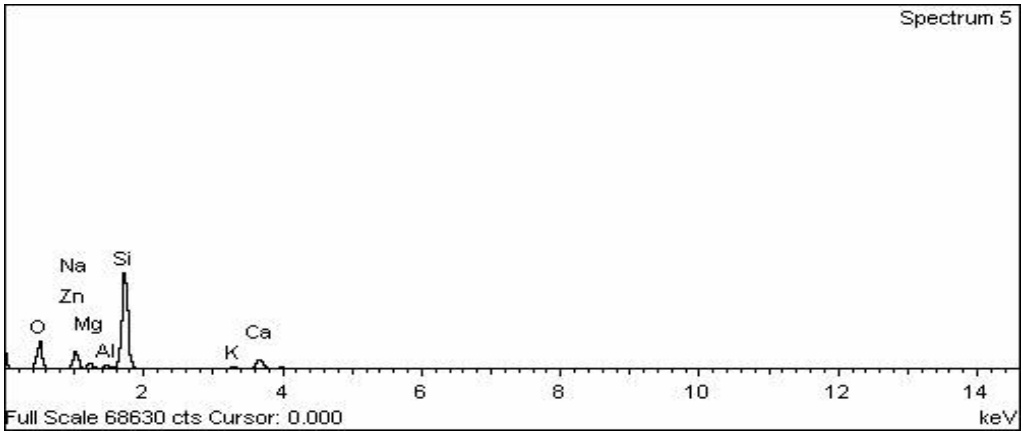

Fig. 22. EDX spectrum of W8100 grown at pH of 8.1.

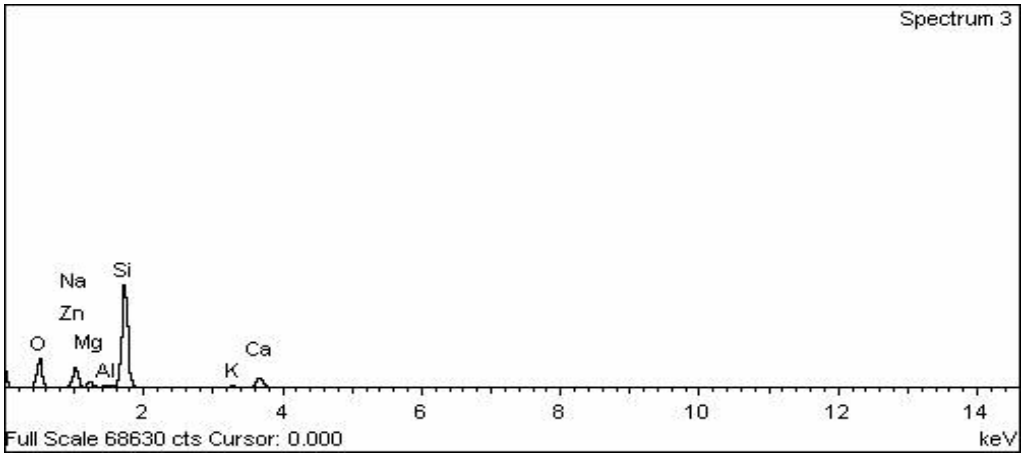

Fig.23. EDX spectrum of W9100 grown at pH of 9.0

The composition by weight of the elements present in both the nanowire and the glass substrate are as shown in the table below:

Table 4. Elemental composition

Element	Weight (%)
Oxygen (O)	36.28
Aluminum (Al)	0.72
Silicon (Si)	26.59
Potassium (K)	0.55
Calcium (Ca)	3.50
Zinc (Zn)	29.16
Sodium (Na)	1.06
Magnesium (Mg)	2.14

The elemental composition from the table above further confirmed the presence of Zinc (29.16%) and Oxygen (36.28%) which is the constituent of Zinc oxide nanowire.

CHAPTER FIVE

5.1. CONCLUSION

This study showed that a well align ZnO nanowire can be grown by chemical bath deposition technique and the normal pH of the bath solution, 8.1 is the optimized value to form ZnO nanowire with top surface of hexagonal shape.

This study further revealed that the crystallite size as well as the absorbance of the nanowire increase with increasing annealing temperature. Its high absorbance in the ultraviolet region suggest that it can be use as solar harvester for trapping solar energy for photovoltaic panel which is capable of converting sunlight radiation directly to electricity for commercial or industrial purpose.

5.2. RECOMMENDATIONS

The production and characterization of ZnO nanowire is of considerable importance to nanotechnology and the world at large due to its unique properties. We therefore recommend the following:

- pH of 8.1 (original bath solution pH) is the optimum pH for the growth of ZnO nanowire with chemical bath deposition method.
- In order to reproduce this result, as a precautionary measure, the substrate on which nanowire is to be grown must be kept free of contamination from bare hands, dust particles etc.
- After the growth, the substrate containing the deposited nanowire must be washed by slowly allowing distilled water from syringe to drop on it and then drip dry in air before annealing.
- Finally, during annealing, the digital temperature regulation oven must first be initialized by setting it to the required temperature and allowing it for some minutes to attain that temperature before the introduction of the nanowire contained in a beaker and then timed.

5.3. REFERENCES

[1]. Hochbaum AI, Yang P. (2010), Semiconductor nanowires for energy conversion, *Chem. Rev.* **110**(1), 527ï 46.

[2]. Fan Z, Ruebusch D.J, Rathore AA, Kapadia R, Ergen O, et al. (2009), Challenges and prospects of nanopillar-based solar cells, *Nano Res.* **2**(11), 829ï 43.

[3]. Xue J, Uchida S, Rand B.P. (2004), Forrest, *Appl. Phys. Lett*., **85**(23), 5757.

[4]. Nuli Y. N, Zhao S. L and Qin Q. Z. (2003), Nanorystalline tin oxides and nickel oxide film anodes for Li-ion batteries, *Power Sources*, **114,** 113-120.

[5]. Nanostructure science and Technology. (1999), R&D Status and Trends in Nanoparticles, Nanostructured Materials and Nanodevices, Kluwer Academic Publishers, chapter 2,7. (http://itri.loyola.edu/nano/final/). Retrieved on 13th May, 2012.

[6]. Xu L. F, Liao Q, Zhang J. P, Ai X. C, and Xu D. S. (2007), Single-crystalline ZnO nanotube arrays on conductive glass substrates by selective dissolution of electrodeposited ZnO nanorods, *J. Phys. Chem. C,* **111**, 4549-4552.

[7]. Jamil Elias, Ramon Tena-Zaera, Guillaume-Yangshu Wang, and Claude Le´vy-Cle´ment, (2008), Conversion of ZnO nanowires into nanotubes with Tailored dimensions, *Chem. Mater*. **20**, 6633-6637.

[8]. Yu Q. J, Fu Y , Yu C. L, Yang H. B, Wei R. H, Li M. H. (2007), Fabrication and optical properties of large-scale ZnO nanotube Bundles via a simple solution route, *J. Phys. Chem. C,* **111**, 17521-17526.

[9]. Tong Y. H, Liu Y. C, Shao C. L, Liu Y. X, Xu C. S, Zhang J. Y. (2006), Growth and optical properties of faceted hexagonal ZnO nanotubes, *J. Phys. Chem. B,* **110**, 14714-14718.

[10]. Xing Y. J, Xi Z. H, Xue Z. Q, Zhang X. D, Song R. M, Wang J. H, Xu J, Zhang S. L, Yua D. P. (2003), Optical properties of the ZnO Nanotubes synthesized via vapor phase growth, *Appl. Phys. Lett.,* **83**, 1689.

[11]. Huang M. H, Mao S, Feick H, Yan H. G., Wu Y.Y, Kind H, Weber E. (2001), Room-temperature ultraviolet nanowire nanolasers, *Science*, **292,** 1897.

[12]. Vayssieres L. (2003), Growth of arrayed nanorods and nanowires of ZnO from aqueous solutions. *Adv. Mater.*, **15**, 464-466.

[13]. Pan Z. W, Dai Z. R, Wang Z. L. (2001), Nanobelts of semiconducting oxides, *Science*, **291**, 1947-1949.

[14]. Wang W. Z, Zeng B. Q, Yang J, Poudel B, Huang J. Y. (2006), Aligned ultralong ZnO nanobelts and their enhanced field emission, *Adv. Mater.,* **18**, 3275-3278.

[15]. Qiu Y, Yang S. (2007), Controlled vapor-phase synthesis and application for humidity sensing, *Adv. Func. Mater.,* **17**, 1345-1352.

[16]. Fuller M. L. (1929), A method of determining the axial ratio of a crystal from X-ray diffraction data: The axial ratio and lattice constants of zinc oxide, *science*, **70**, 196.

[17]. Lee J. S, Park K, Kang M. I, Park I. W, Kim S. W, Chom W. K. (2003), ZnO nanomaterials synthesized from thermal evaporation of ballmilled ZnO powders, *J. Cryst. Growth,* **254**, 423-431.

[18]. Sun Y, Fuge G. M, and Ashfold M. N. R. (2004), Growth of aligned ZnO nanorod arrays by catalyst-free pulsed laser deposition methods, *Chem. Phys. Lett.,* **396**, 21-26.

[19]. Wu J, Liu S. C. (2002), Low-temperature growth of well-aligned ZnO nanorods by chemical vapor deposition, *Adv .Mater.*, **14**, 215-218.

[20]. Vayssieres L, Keis K, Lindquist S. E, Hagfeldt A. (2001), Purpose-built anisotropic metal oxide material:3D highly oriented microrod array of ZnO, *J. Phys. Chem. B*, **105**, 3350-3352.

[21]. Lu Y et al. (2010), Cold welding of ultrathin gold nanowires, *Nature Nanotechnology*, **5**, 213-224.

[22]. Li, Q. H. et al. (2004), Oxygen sensing characteristics of individual ZnO nanowire transistors, *Applied Physics Letters*, ***85***(26), 4289-4291.

[23]. Zhang, D. et al. (2003), Doping dependent NH_3 sensing of indium oxide nanowires. *Applied Physics Letters*, *83*(9), 1845-1847.

[24]. Kind, H. (2002), Nanowire ultraviolet photodetectors and optical switches. *Advanced Materials*, **14**(2), 137-139.

[25]. Cui, Y., Wei Q., Park, H., & Lieber, C. (2001), Nanowire nanosensors for highly sensitive and selective detection of biological and chemical species. *Science*, ***293***, 1289-1292.

[26]. Look, D.C., Hemsky J.W., and Sizelove J.R.. (1999), *Residual Native Shallow Donor in ZnO.* PHysical Review Letters. **82**(12), 2552.

[27]. Reynolds, D.C., Look D.C and Jogai B. (1999), Optically pumped ultraviolet lasing from ZnO. *Solid State Communication,* **99**(12), 873-875.

[28]. Lu Y, Huang J, Wang C, Sun S, Lou J. (2010), Cold welding of ultrathin gold nanowires, *Nature Nanotechnology,* **5**, 218 ï 224.

[29]. Grange R, Choi J.W, Hsieh C.L, Pu Y, Magrez, A. (2009), Lithium niobate nanowires: synthesis, optical Properties and manipulation, *Applied Physics Letters,* **95**, 143105.

[30]. Thurn-Albrecht T et al. (2000), Ultrahigh-density nanowire arrays grown in self-assembled diblock copolymer templates, *Science*, **290,** 2126.

[31]. Nielsch K, Wehrspohn R B, Fischer S F, Kronmiller H, Kirsehner J. (2001), Nanowires: properties, applications and synthesis via porous anodic aluminium oxide template, *Mater. Res. Soc. Symp. Proc.* **9**, 426.

[32]. Gudiksen M. S, Lauhon L. J, Wang J, Smith D. C. (2002), Growth of nanowire superlattice, *Nature*, **415**, 407.

[33]. Lei Liao, Yung-Chen Lin, Mingqiang Bao, Rui Cheng, Jingwei Bai, Yuan Liu, Yongquan Qu, Kang L. Wang, Yu Huang, & Xiangfeng Duan. (2010), High-speed graphene transistors with a self-aligned nanowire gate, *Nature*, **467**, 305-8.

[34]. Duan X, Niu C, Sahi V, Chen J, Parce J. W, Empedocles S, and Goldman, J. (2003), High performance thin film transistors assembled from semiconductor nanowires and nanoribbons, *Nature,* **425**, 274-278.

[35]. Chung S W, Yu J Y and Heath J R. (2000), Silicon Nanowires:ز Preparation, device fabrication, and transport properties, *J. Phys. Chem. B*, **55**, 2047.

[36]. Johnson J C, Choi H J, Knutsen K P, Schaller R D, Yang P.(2002), Single gallium nitride nanowire lasers, *Nature Mater*., **1**, 106-10.

[37]. Huynh W U, Dittmer J J and Alivisatos A P.(2002), Hybrid nanorod-polymer solar cells, *Science,* **295**, 2425.

[38]. Lee J.D. (1991), *Concise inorganic chemistry*, fourth ed. Chapman & Hall, London, 845.

[39]. Harris, P.F.J. (2002), *Carbon nanotubes and related structures* (1st.ed.). Cambridge University Press, pp. 213ï 32.

[40]. Pauling L (1930), The Structure of the Chlorites*, Proc. Natl. Acad. Sci. U.S.A,* **16**(9), 578ï 82.

[41]. Tenne R, Margulis L, Genut M, Hodes G (1992), Polyhedral and cylindrical structures of tungsten disulphide, *Nature* **360** (6403), 444ï 446.

[42]. Zak A, Sallacan L, Fleischer N and Tenne R. (2011), large-scale synthesis of WS_2 multiwall nanotubes, *J. Sensors& Transducers,* **12**(10), 1ï 10.

[43]. Na S.I, Kim S.S, Hong W. K, Park J.W, Jo J, Nah Y.C, Lee T, Kim D.Y. (2008), Fabrication of TiO_2 nanotubes by using electrodeposited ZnO nanorod template and their application to hybrid solar cells, *Electrochimica Acta* **53** (5), 2560.

[44]. Kis A, Mihailovic D, Remskar M, Mrzel A, Jesih A, Piwonski I, Kulik A. J, Benoit W, Forro L. (2003), Shear and Young's Moduli of MoS_2 Nanotube Ropes, *Advanced Materials,* **15** (9), 733.

[45]. Kreizman R, Enyashin A. N, Deepak F. L, Albu-Yaron A, Popovitz-Biro R, Seifert G and Tenne R. (2010), Synthesis of Core-Shell Inorganic Nanotubes, *Adv. Funct. Mater.,* **20** (15), 2459ï 2468.

[46]. Krause M, Mucklich A, Zak A, Seifert G and Gemming S. (2011), High resolution TEM study of WS_2 nanotubes, *Phys. Status Solidi B* **248** (11), 2716ï 2719.

[47]. Zhu Y. Q, Kroto H. W. (2003), Shock-wave resistance of WS_2 Nanotubes, *J. Am. Chem. Soc.,* **125** (5), 1329ï 1333.

[48]. Wang, X. *et al.* (2009), Fabrication of ultralong and electrically uniform Single-walled Carbon nanotubes on clean substrates, *Nano Letters,* **9** (9), 3137ï 3141.

[49]. Martel, R. *et al.* (2001), Ambipolar electrical transport in semiconducting single-wall carbon nanotubes, *Physical Review Letters,* **87** (25), 256805.

[50]. Zavalniuk V, Marchenko S. (2011), Theoretical analysis of telescopic oscillations in multi-walled carbon nanotubes, *Low temperature Physics*, **37** (4), 337.

[51]. Flahaut E, Bacsa R, Peigney A, Laurent C. (2003), Gram-scale CCVD Synthesis of Double-Walled Carbon Nanotubes, *Chemical Communications*, **12**(12), 1442ï 1443.

[52]. Berkeley Lab. (2009), A Better Way to Make Nanotubes http://newscenter.lbl.gov/feature-stories/2009/01/05/better-way-to-make-nanotubes/. Retrieved on 13th may, 2012.

[53]. Guan L, Suenaga K, Iijima S. (2008), Smallest carbon nanotube assigned with atomic resolution accuracy, *Nano Letters.,* **8** (2), 459ï 462.

[54]. Yu, Min-Feng, Lourie, Oleg, Dyer, Mark J, Moloni, Katerina, Kelly, Thomas F, Ruoff, Rodney S. (2000), Strength and breaking mechanism of multi-walled carbon nanotubes under tensile load, *Science,* **287** (5453), 637ï 640.

[55]. Peng B, Locascio M, Zapol P, Li S, Mielke S. L, Schatz G. C, and Espinosa H. D. (2008), Measurements of near-ultimate strength for multiwalled carbon nanotubes and irradiation-induced crosslinking improvements, *Nature Nanotechnology*, **3**, 626 ï 631.

[56]. Jensen K, Mickelson W, Kis A and Zettl A. (2007), Buckling and kinking force measurements on individual multi-walled carbon nanotubes, *Phys. Rev. B* **76**, 195436.

[57]. Popov M. *et al.* (2002), Superhard phase composed of single-wall carbon nanotubes, *Phys. Rev. B* **65** (3), 033408.

[58]. Huhtala M, Kuronen A, Kaski K. (2002), Carbon nanotube structures: Molecular dynamics simulation at realistic limit, *Computer Physics Communications,* **146**, 30.

[59]. Pop, Eric, Mann, David, Wang, Qian, Goodson, Kenneth, Dai, Hongjie. (2005), Thermal conductance of an individual single-wall carbon nanotube above room temperature, *Nano Letters* **6** (1), 96ï 100.

[60]. Sinha, Saion *et al.* (2005), Off-axis thermal properties of carbon nanotube films, *Journal of Nanoparticle Research* **7** (6), 651ï 657.

[61]. Ebbesen T, Ajayan W. (1992), Large-scale synthesis of carbon nanotubes, *Nature,* **358** (6383), 220ï 222.

[62]. Collins, PHilip G. (2000), Nanotubes for Electronics, *Scientific American*, **67**, 69.

[63]. Inami N et al. (2007), Synthesis-condition dependence of carbon nanotube growth by alcohol catalytic chemical vapor deposition method, *Sci. Technol. Adv. Mater.*, **8**, 292.

[64]. Eftekhari A, Jafarkhani P, Moztarzadeh F. (2006), High-yield synthesis of carbon nanotubes using a water-soluble catalyst support in catalytic chemical vapor deposition, *Carbon* **44** (7), 1343.

[65]. Boyd, Jade. (2006), Rice chemists create, grow nanotube seeds, Rice University. http://www.media.rice.edu/media/NewsBot.asp?MODE=VIEW&ID=9070. Retrieved on 13th may, 2012.

[66]. Manias, Evangelos. (2007), Nanocomposites: Stiffer by design, *Nature Materials,* **6** (1), 9ï 11.

[67]. Motta, M. *et al.* (2007), High Performance Fibres from 'Dog Bone' Carbon nanotubes, *Advanced Materials,* **19** (21), 3721ï 3726.

[68]. "New Flexible Plastic Solar Panels Are Inexpensive And Easy To Make". ScienceDaily.July 19,2007. http://www.sciencedaily.com/releases/2007/07/070719011151.htm. Retrieved on 13th may 2012.

[69]. Sowinski S, Jolly C, Berninghausen O et al. (2008), Membrane nanotubes physically connect T cells over long distances presenting a novel route for HIV-1 transmission, *Nat. Cell Biol.* **10** (2), 211ï 9.

[70]. Onfelt B, Nedvetzki S, Benninger R.K et al. (2006), Structurally distinct membrane nanotubes between human macrophages support long-distance vesicular traffic or surfing of bacteria, *J. Immunol.* **177** (12), 8476ï 83.

[71]. Belting M, Wittrup A. (2008), Nanotubes, exosomes, and nucleic acidï binding peptides provide novel mechanisms of intercellular communication in eukaryotic cells: implications in health and disease, *J. Cell Biol.* **183** (7), 1187ï 91.

[72]. Ramírez-Weber FA, Kornberg TB. (1999), Cytonemes: cellular processes that project to the principal signaling center in Drosophila imaginal discs, *Cell* **97** (5), 599ï 607.

[73].Onfelt B, Nedvetzki S, Yanagi K, Davis DM. (2004), Cutting edge: Membrane nanotubes connect immune cells, *J. Immunol.,* **173** (3), 1511ï 3.

[74].http://medgadget.com/2010/03/breakthrough_in_dna_nanotube_research.html. Retrieved on 6th feb., 2012.

[75]. Ajayan P.M, Schadler L.S, Braun P.V. (2003), *Nanocomposite science and technology*, Wiley.

[76]. Kamigaito, O. (1994). What can be improved by nanometer composites?, *J. Jpn. Soc*., **38**:315-21.

[77]. Kruis F. E, Fissan H and Peled A. (1998), Synthesis of nanoparticles in the gas phase for electronic, optical and magnetic applications ï a review, *J. Aerosol Sci.,* **29** (5ï 6), 511ï 535.

[78]. Zhang S, Sun D, Fu Y, and Du H. (2003), Recent advances of superhard nanocomposite coatings: a review, *Surf. Coat. Technol.,* **167** (2ï 3), 113ï 119.

[79]. Birkholz M, Albers U and Jung T. (2004), Nanocomposite layers of ceramic oxides and metals prepared by reactive gas-flow sputtering, *Surf. Coat. Technol.* **179** (2ï 3), 279ï 285.

[80]. Bakshi S. R, Lahiri D, and Argawal A. (2010), *Carbon nanotube reinforced metal matrix composites - A Review*, International Materials Reviews, vol. 55. http://web.eng.fiu.edu/agarwala/PDF/2010/12.pdf. Retrieved on 14th may, 2012.

[81]. Manias Evangelos. (2007), Nanocomposites: Stiffer by design, *Nature Materials,* **6** (1), 9ï 11.

[82].Usuki, Arimitsu, Kojima, Yoshitsugu, Kawasumi, Masaya, Okada, Akane, Fukushima, Yoshiaki; Kurauchi, Toshio, Kamigaito, Osami. (1993), Synthesis of nylon 6-clay hybrid, *Journal of Materials Research,* **8** (5), 1179.

[83]. Professor Hay J.N and Shaw S.J. (2000), ñA Review of Nanocompositesôô. http://www.cem.msu.edu/~kanatzid/Nanocomposites.html. Retrieved on 17th feb., 2012.

[84]. Sing, K. S, Everett W, Haul D. H, Moscou R. A. W, Pierotti L, Rouquerol R. A, Siemieniewska T. (1984), Reporting physisorption data for gas/solid systems with special reference to the determination of surface area and porosity, *Pure and Applied Chemistry* **57**, 603-19.

[85]. Lu G. Q, & Zhao X. S. (2004), Nanoporous materials- an overview, *Series on Chemical Engineering,* **4**, 1-13.

[86]. Lin, Y.W, Huang, M. F. & Chang H.T. (2005), .Nanomaterials and chip-based nanostructures for capillary electrophoretic separations of DNA, *Electrophoresis* **26**, 320-330.

[87]. Shi J, Zhu Y, Zhang X, Baeyens W. R. G. & Garcia-Campana A. M. (2004), Recent developments in nanomaterial optical sensors. *TrAC, Trends in Analytical Chemistry,* **23**, 351-360.

[88]. Kresge, C. T, Leonowicz, M. E, Roth W. J, Vartuli J. C & Beck J. S. (1992), Ordered mesoporous molecular-sieves synthesised by a liquid-crystal template mechanism, *Nature ,* **359,** 710ï 712.

[89]. Yang P. D, Zhao D. Y, Margolese D. I, Chmelka B. F. & Stucky G. D. (1998), Generalized syntheses of large-pore mesoporous metal oxides with semicrystalline frameworks, *Nature,* **396,** 152ï 155.

[90]. Grosso, D. *et al*. (2005), Periodically ordered nanoscale islands and mesoporous films composed of nanocrystalline multimetallic oxides, *Nature Mater.,* **3,** 787ï 792.

[91]. Deshpande A. S, Pinna N, Smarsly B, Antonietti, M. & Niederberger, M. (2005), Controlled assembly of preformed ceria nanocrystals into highly ordered 3D nanostructures, *Small,* **1**, 313ï 316.

[92]. Ba J. H, Polleux J, Antonietti M & Niederberger M. (2005), Non-aqueous synthesis of tin oxide nanocrystals and their assembly into ordered porous mesostructures, *Adv. Mater.,* **17**, 2509ï 2512.

[93]. Brinker, C. (1990), *Sol-gel science,* Academic Press, New York, N. Y.

[94]. Hench, L. L. (1998), *Sol-Gel Silica: Properties, Processing and Technology Transfer,* Noyes, Westwood, N. J.

[95]. Beck J. S, Vartuli J. C, Roth, W. J, Leonowicz M. E, Kresge C. T, Schmitt K. D, Chu, C. T. W, Olson D. H, Sheppard E. W. (1992), A new family of mesoporous molecular sieves prepared with liquid crystal templates, *Journal of the American Chemical Society,* **114**, 10834-43.

[96]. Wei Y, Jin D. L, Ding T. Z, Shih W. H, Liu X. H, Cheng S. Z. D. & Fu Q. (1998), A non-surfactant templating route to mesoporous silica materials, *Advanced Materials,* **10**, 313-316.

[97].Wei Y, Xu J, Dong H, Dong J. H, Qiu K & Jansen-Varnum S. A. (1999), Preparation and physisorption characterization of D-glucose-templated mesoporous silica sol-gel materials, *Chemistry of Materials,* **11**, 2023-2029.

[98].Boennemann H & Nagabhushana K. S. (2004), Chemical synthesis of nanoparticles, *Encyclopedia of Nanoscience and Nanotechnology,* **1**, 777-813.

[99].Ying J. Y, Mehnert C. P. & Wong M. S. (1999), Synthesis and applications of supramolecular-templated mesoporous materials, *Angew. Chem. Int. Edn.,* **38,** 56ï 77.

[100].Wang Z. L. (2004), Inorganic Nanoparticles: Synthesis, Applications, and Perspectives, *Annu. Rev. Phys. Chem*. ***55***, 159-196.

[101]. Xiang B, Wang P, Zhang X, Dayeh S. A, Aplin D. P. R, Soci C, Yu D, Wang, D.(2007), ZnO nanowire based visible-transparent ultraviolet detectors on polymer substrates, *Nano Lett.* **7**, 323-328.

[102].Ohgaki T, Ohashi N, Kakemoto H, Wada S, AdachiY, Haneda H, Tsurumi T.(2003), Synthesis of ZnO nanowires *and* applications as gas sensors, *J. Appl. Phys.* **93**, 1961-1965.

[103]. Sun Y, Fuge G. M, Fox N. A, Riley D. J, Ashfold M. N. R. (2005), Low-temperature solution growth of ZnO nanotube arrays, *Adv. Mater.***17**, 2477-2481.

[104]. Ding Y, Wang Z. L. *J.* (2004), Enhanced Ultraviolet Emission from ZnS-Coated ZnO Nanowires Fabricated by Self-Assembling Method *Phys. Chem. B*, **108**, 12280-12291.

[105].Niesen, T. P.; De Guire, M. R. (2001), Particle growth and particleï surface interactions during low-temperature deposition of ceramic thin films, *J . Electroceram.*, **6**, 169.

[106].Boyle D.S, Bayer A, Heinrich M.R, Robbe O, Brien P.O. (2000), Characterization of ZnO thin films grown by chemical bath deposition, Thin Solid Films, **150**, 361.

[107]. Izaki, M. (2002), Light-assisted chemical deposition of highly (0001) oriented zinc oxide film, *Chem. Commun*.**4**, 476.

[108]. Govender K, Boyle D. S, Kenway P. B, OôBrien P.(2004), Phase transformation and resistivity of dumbbell-like ZnO microcrystals under high pressure, *J. Mater. Chem. **14***, 2575.

[109].Yang L.L et al. (2008), Zinc oxide nanowire; controlled low temperature growth & some electrochemical and optical devices. http//pub.isb.org

[110]. Greene L. E, Yuhas B. D, Law M, Zitoun D, Yang, P. (2006), ZnO Nanotube Based Dye-Sensitized Solar Cells, *Inorg. Chem.* **45**, 7535-7543.

[111]. Lincot, D. (2005), electrochemical growth of $CuInSe_2$ thin film on different substrate from alkaline medium, *Thin Solid Films*, **487**, 40-48.

[112]. Cao G, Liu, D. (2008), electrophoretic deposition of nanomaterials, *Adv. Colloid Interface Sci.* **136**, 45-64.

[113].Vayssieres L, Keis K, Lindquist S.E and Hagfeldt A. (2001), Purpose-built anisotropic metal oxide material: 3d highly oriented microrod array of ZnO, *J. Phys. Chem. B*, **105**(17), 3350-3352.

[114]. Izaki M, Shinoura, O.(2001) , Aqueous Solution Preparation, Structure, and Magnetic Properties of Nano-Granular $Zn_xFe_{3-x}O_4$ Ferrite Films, *Adv. Mater.*, ***13***, 142

5.4. **APPENDIX**

36-1451 Quality: Quality Data

Zn O Zinc Oxide Zincite, Syn				
Rad:CuKa1	Lambda:1.540598	Filter:Monochromator crystal used		d sp:Diffractometer
Cutoff:	Int:Diffractometer	I/Icor:		
Ref:McMurdie, H., Morris, M., Evans, E.,Paretzkin, B., Wong-Ng, W., Ettlinger, L.,Hubbard, C.1. Bragg, W.2. Abrahams, S., Berr				
Sys:Hexagonal		S.G.:P63mc		
a:3.24982±9E-5	b:	c:5.20661±0.00015		
α:	β:	γ:	Z:2	mp
Ref2				
Dx:	Dm:5.675	SS/FOM: F27=130.8(0.0071,29)		Volume[CD]:47.62
εα:	ηωβ:2.013	εγ:2.029	Sign:+	2V:
Ref3				
Color:Colorless				
The sample was obtained from the New Jersey Zinc Co., Bethlehem, PA, USA. The structure was determined by Bragg (1) and refined by Abrahams, Bernstein (2). A high pressure cubic NaCl-type of ZnO is reported by Bates et al. (3) and a cubic, sphalerite type is reported by Radczewski, Schicht (4). The approximate temperature of data collection was 26 C. To replace 5-664 (5). References to other early patterns may be found in reference (5).				

27 reflections in pattern. Wavelength 1.5406 was used to calculate the diffraction angles.

2θ	Int.	h k l	2θ	Int.	h k l	2θ	Int.	h k l	2θ	Int.	h k l
31.7702	57	1 0 0	76.9551	4	2 0 2	116.2792	8	2 1 3			
34.4220	44	0 0 2	81.3703	1	1 0 4	121.5722	4	3 0 2			
36.2531	100	1 0 1	89.6074	7	2 0 3	125.1884	1	0 0 6			
47.5390	23	1 0 2	92.7839	3	2 1 0	133.9321	3	2 0 5			
56.6032	32	1 1 0	95.3040	6	2 1 1	136.5205	1	1 0 6			
62.8647	79	1 0 3	98.6177	4	1 1 4	138.5133	2	2 1 4			
66.3802	4	2 0 0	102.9462	2	2 1 2	142.9185	3	2 2 0			
67.9630	23	1 1 2	104.1342	5	1 0 5						
69.1002	11	2 0 1	107.4302	1	2 0 4						
72.5621	2	0 0 4	110.3922	3	3 0 0						

Fig.24 Compound phase of W8150

36-1451 Quality: Quality Data

Zn O
Zinc Oxide
Zincite, Syn

Rad:CuKa1 Lambda:1.540598 Filter:Monochromator crystal used d sp:Diffractometer
Cutoff: Int:Diffractometer I/Icor:
Ref:McMurdie, H., Morris, M., Evans, E.,Paretzkin, B., Wong-Ng, W., Ettlinger, L.,Hubbard, C.1. Bragg, W.2. Abrahams, S., Berr

Sys:Hexagonal S.G.:P63mc
a:3.24982±9E-5 b: c:5.20661±0.00015
α: β: γ: Z:2 mp
Ref2
Dx: Dm:5.675 SS/FOM: F27=130.8(0.0071,29) Volume[CD]:47.62

εα: ηωβ:2.013 εγ:2.029 Sign:+ 2V:
Ref3

Color:Colorless

The sample was obtained from the New Jersey Zinc Co., Bethlehem, PA, USA. The structure was determined by Bragg (1) and refined by Abrahams, Bernstein (2). A high pressure cubic NaCl-type of ZnO is reported by Bates et al. (3) and a cubic, sphalerite type is reported by Radczewski, Schicht (4). The approximate temperature of data collection was 26 C. To replace 5-664 (5). References to other early patterns may be found in reference (5).

27 reflections in pattern. Wavelength 1.5406 was used to calculate the diffraction angles.

2 θ	Int.	h	k	l	2 θ	Int.	h	k	l	2 θ	Int.	h	k	l	2 θ	Int.	h	k	l
31.7702	57	1	0	0	76.9551	4	2	0	2	116.2792	8	2	1	3					
34.4220	44	0	0	2	81.3703	1	1	0	4	121.5722	4	3	0	2					
36.2531	100	1	0	1	89.6074	7	2	0	3	125.1884	1	0	0	6					
47.5390	23	1	0	2	92.7839	3	2	1	0	133.9324	3	2	0	5					
56.6032	32	1	1	0	95.3040	6	2	1	1	136.5205	1	1	0	6					
62.8642	29	1	0	3	98.6127	4	1	1	4	138.5133	2	2	1	4					
66.3802	4	2	0	0	102.9462	2	2	1	2	142.9185	3	2	2	0					
67.9630	23	1	1	2	104.1342	5	1	0	5										
69.1002	11	2	0	1	107.4302	1	2	0	4										
72.5621	2	0	0	4	110.3922	3	3	0	0										

Fig.25 Compound phase of W8200